

1 The roles of climate, geography and natural selection as drivers of genetic and phenotypic differentiation  
2 in a widespread amphibian *Hyla annectans* (Anura: Hylidae)

3 Shichao Wei<sup>1</sup>, Zitong Li<sup>2</sup>, Paolo Momigliano<sup>2</sup>, Chao Fu<sup>1</sup>, Hua Wu<sup>1\*</sup>, & Juha Merilä<sup>2</sup>

4

5 <sup>1</sup>Institute of Evolution and Ecology, School of Life Sciences, Central China Normal University, 152  
6 Luoyulu, Hongshan District, 430079 Wuhan, China

7 <sup>2</sup>Ecological Genetics Research Unit, Organismal and Evolutionary Biology Research Programme,  
8 Faculty of Biological and Environmental Sciences, University of Helsinki, P.O. Box 65, FI-00014  
9 Helsinki, Finland

10 **Corresponding author:** Hua Wu (wuhua@mail.ccnu.edu.cn, Telephone: 86-027-67867021; fax:86-  
11 027-67861147); Institute of Evolution and Ecology, School of Life Sciences, Central China Normal  
12 University, 152 Luoyulu, Hongshan District, 430079 Wuhan, China

13

14 **Running title:** Phylogeography of *Hyla annectans*

15

16 **Abstract**

17 The role of geological events and Pleistocene climatic fluctuations as drivers of current patterns of  
18 genetic variation in extant species has been a topic of continued interest among evolutionary biologists.  
19 Nevertheless, comprehensive studies of widely distributed species are still rare, especially from Asia.  
20 Using geographically extensive sampling of many individuals and a large number of nuclear single  
21 nucleotide polymorphisms (SNPs), we studied the phylogeography and historical demography of *Hyla*  
22 *annectans* populations in southern China. Thirty-five sampled populations were grouped into seven  
23 clearly defined genetic clusters that closely match phenotype-based subspecies classification. These  
24 lineages diverged 2.32–5.23 million years ago, a timing that closely aligns with the rapid and drastic  
25 uplifting of the Qinghai-Tibet Plateau and adjacent southwest China. Demographic analyses and species  
26 distribution models indicate that different populations of this species have responded differently to past  
27 climatic changes. In the Hengduan Mountains, most populations experienced a bottleneck, whereas the  
28 populations located outside of the Hengduan Mountains have gradually declined in size since the end of  
29 the last glaciation. In addition, the levels of phenotypic and genetic divergence were strongly correlated  
30 across major clades. These results highlight the combined effects of geological events and past climatic  
31 fluctuations, as well as natural selection, as drivers of contemporary patterns of genetic and phenotypic  
32 variation in a widely distributed anuran in Asia.

33 **Keywords:** phylogeography, climatic fluctuations, population divergence, SNP, natural selection

## 34 **Introduction**

35 Contemporary patterns of genetic variation across different geographic areas are affected by historical  
36 factors (Avice 1994; Hewitt 2004). Geological events such as the formation of mountain ranges and  
37 river systems can generate physical barriers to dispersal, fragmenting once connected habitats, hence  
38 resulting in allopatric divergence and speciation (Che *et al.* 2010; Chaves *et al.* 2011). Past climatic  
39 fluctuations, particularly those during the late Pleistocene, were important drivers of current  
40 distributions, genetic diversification, and demographic fluctuations of many temperate species and  
41 communities (Hewitt 2000; Hewitt 2004). During glacial periods, many taxa retreated into refugia and  
42 subsequently underwent range expansions during postglacial periods in response to the availability of  
43 newly formed habitats (Hewitt 2004). Hence, contemporary patterns of genetic variation within  
44 temperate zone species have been likely influenced by both paleogeological events and Pleistocene  
45 climatic fluctuations (Hewitt 1996; Kumar & Kumar 2018; Li *et al.* 2018).

46 Genetic methods have been widely used to investigate the effects of climate and geography in driving  
47 current patterns of genetic and phenotypic variation within species (Avice 2000; Hewitt 2000; Leinonen  
48 *et al.* 2013; Kumar & Kumar 2018). Phylogeographic studies were initially based on mitochondrial  
49 DNA (mtDNA; Avice *et al.* 1987), and subsequently complemented with nuclear markers (e.g. Yan *et al.*  
50 *et al.* 2013; Li *et al.* 2018). Given the now well-known limitations of evolutionary inferences based on  
51 mtDNA (Avice 2000; Ballard & Whitlock 2004; Guo *et al.* 2019), next generation sequencing (NGS)  
52 methods have largely replaced mtDNA and microsatellite markers in phylogeographic and population  
53 genetic investigations of non-model organisms (Avice 2009; McCormack *et al.* 2013). Although  
54 phylogeographic studies using NGS data have become increasingly common, most have focused on  
55 European and North American areas (e.g. Newman & Austin 2016; Dufresnes *et al.* 2019), while large-  
56 scale phylogeographic studies based on NGS data from Asia are still relatively rare (but see: Zhao *et al.*  
57 2013; Zhou *et al.* 2016; Puckett *et al.* 2016; Jiang *et al.* 2018; Wang *et al.* 2018; Feng *et al.* 2019)

58 Southern China provides an interesting area for phylogeographic studies due to its unique geophysical  
59 conditions and abundant biodiversity (Yan *et al.* 2013; Li *et al.* 2015b; Li *et al.* 2018). The geological  
60 features of Chinese mainland have been remodeled by the uplift of the Himalayas and the Qinghai-Tibet  
61 Plateau (QTP; Harrison *et al.* 1992; Zhang 1999). Presently, these areas are characterized by many high-  
62 elevation mountains, plateaus and river systems such as the Hengduan Mountains, Yunnan-Guizhou  
63 Plateau, and Yangtze River (Zhang 1999). These geographic barriers have likely played important roles  
64 in driving the genetic and phenotypic divergence of the species native to this region (Che *et al.* 2010;  
65 Yan *et al.* 2013). Over the East Asian continent temperatures during the LGM were 2–4 °C colder than  
66 today (Weaver *et al.* 1998; Ju *et al.* 2007), but unlike in Europe and North America, most areas in  
67 southern China were not covered by ice sheets during the Pleistocene (Shi *et al.* 1986; Liu 1988) – with  
68 the exception of the Hengduan Mountains (Zheng *et al.* 2002). Thus, Quaternary climatic fluctuations  
69 might have had less impact on patterns of genetic variation in southern China compared to Europe and  
70 North America, and their impact within regions of Southern China might have been heterogeneous  
71 (Wang & Ge 2006; Gao *et al.* 2011; Yan *et al.* 2013).

72 Amphibians have been identified as good models for studying the factors that shape the patterns of  
73 genetic variation and differentiation, mainly for two reasons. First, because of their limited dispersal  
74 ability, they display very high levels of population genetic structuring compared to other animal classes  
75 (Ward *et al.* 1992; Zeisset & Beebee 2008; Sánchez-Montes *et al.* 2018). Second, as ectotherms they  
76 are sensitive to climatic conditions, and are thereby considered to be good indicators of climate change,  
77 both past and present (Bossuyt & Milinkovitch 2001; Graham *et al.* 2004; Kozak & Wiens 2010).

78 The Jerdon's tree frog *Hyla annectans* (Anura: Hylidae) is widely distributed in Asia south of the  
79 Himalayas. In southern China, it occurs in low-to-medium elevation (ca. 580–2,500 m above sea level)  
80 forests (Fei *et al.* 2009). Currently, five subspecies (*viz.* *H. a. gongshanensis*, *H. a. tengchongensis*, *H.*  
81 *a. jingdongensis*, *H. a. chuanxiensis*, and *H. a. wulingensis*) with disjunct geographic distributions are  
82 recognized (Fei *et al.* 2009). The subspecies display phenotypic divergence in number and shape of



83 black spots on their flanks (Fei *et al.* 2009): such divergence indicates that these traits may have been  
84 subject to divergent sexual and/or natural selection. Given that the most recent common ancestor  
85 (MRCA) of *H. annectans* dates back to the mid Pliocene (~4 Mya, 95% CI: 3–5 Mya; Li *et al.* 2015a),  
86 the species has been exposed to the intense uplift of the Qinghai-Tibetan Plateau (QTP) and adjacent  
87 southwest China (Cui *et al.* 1996; Sun *et al.* 2011) and subsequent climatic oscillations. Hence, it is an  
88 ideal amphibian model system to study the effects of past geomorphological events and historical  
89 climatic fluctuations on phylogeography and historical demography.

90 The primary aim of this study was to investigate the impacts of the past geomorphological events and  
91 Pleistocene climatic fluctuations on the patterns of genomic differentiation and historical demography  
92 in *H. annectans*. We screened thousands of genome wide genetic markers in a large number of samples  
93 covering most of the species distribution area in China, and subjected the data to various population  
94 genomic analyses, species distribution modelling, as well as analyses of historical demography. In  
95 addition, we tested for effects of natural selection on phenotypic traits, and whether the levels of  
96 (presumably neutral) genetic divergence among populations predicts levels of phenotypic divergence.  
97 Hence, the results were expected to yield insights as to how past geological events, climatic fluctuations  
98 and natural selection have shaped the distribution of genetic and phenotypic variation in an amphibian  
99 distributed over a large geographic area.

## 100 **Materials and methods**

### 101 **Sampling and DNA extractions**

102 The sample collection of *H. annectans* was planned based on the maps provided in Fei *et al.* (2009). In  
103 total, we obtained 349 samples from 35 sites collected throughout the species' distribution range in  
104 China (Figure 1, Table S1). Ten adult specimens per site were collected, with the exception of location  
105 "20", from where nine specimens were obtained (Table S1). Muscle tissue was taken from each  
106 specimen and preserved in 99% ethanol in the field, and later transferred to a -20 °C freezer in the

107 Molecular and Behavioral Ecology Research Group Laboratory, Central China Normal University,  
108 Wuhan. Genomic DNA was extracted using a standard CTAB protocol (Hanania *et al.* 2004). DNA  
109 concentration and quality were assessed using a ND-1000 spectrophotometer (NanoDrop, Wilmington,  
110 DE, USA); DNA quality was also checked on 1% agarose gels with lambda DNA standard.

### 111 **High-throughput sequencing and single nucleotide polymorphism data assembly**

112 We used the high-resolution Specific Length Amplified Fragment Sequencing (SLAF-seq) strategy for  
113 large-scale *de novo* SNP discovery and genotyping (Sun *et al.* 2013). The genome of *Xenopus tropicalis*  
114 (GenBank assemble accession: GCA\_000004195.2) was chosen as a reference for running an *in silico*  
115 digestion to determine an appropriate combination of restriction enzymes. Appropriate enzymes should  
116 result in a large number (> 100,000) of unique SLAF markers that are randomly distributed throughout  
117 the training genome and contain a low proportion of repeat sequences. Based on the training results, we  
118 chose a combination of *HaeIII* and *Hpy166II* (New England Biolabs, NEB) restriction enzymes with a  
119 size-selection window of 414–444 bp, which was expected to yield approximately 110,000 SLAF tags  
120 in *X. tropicalis*. These enzymes were used to digest the genomic DNA of *H. annectans* for SLAF-seq  
121 library construction. Genomic DNA of each sample was digested with *HaeIII* and *Hpy166II* (New  
122 England Biolabs, NEB), and a dATP was used to add a single nucleotide (A) with Klenow Fragment  
123 (3'→5' exo-) (NEB). Duplex Tag-labeled Sequencing adapters (PAGE purified, Life Technologies,  
124 USA) were ligated using T4 Ligase to the A-tailed DNA. The PCR reactions were run using diluted  
125 restriction-ligation samples, dNTPs, Q5® High-Fidelity DNA Polymerase, and forward (5'-  
126 AATGATACGGCGACCACCGA-3') and reverse (5'-CAAGCAGAAGACGGCATAACG-3'; PAGE  
127 purified, Life Technologies, Beijing) primers. PCR products were purified using Agencourt AMPure  
128 XP beads (Beckman Coulter, High Wycombe, UK) and pooled. The pooled samples were checked by  
129 electrophoresis in a 2% agarose gel, and fragments varying in length from 414 to 444 bp (with indices  
130 and adaptors) were isolated using a Blue Pippin (Sage Science, Beverly, MA). The purified products

131 were submitted for paired-end 100-bp sequencing on the Illumina HiSeq 2500 system (Illumina, Inc;  
132 San Diego, CA, USA) according to the manufacturer's guidelines.

### 133 **Data processing and SNP calling**

134 Adaptor contamination, primer contamination, and low quality reads were present in the raw sequence  
135 reads. FastQC (<http://www.bioinformatics.babraham.ac.uk/projects/fastqc/>) was used to run an initial  
136 quality check on the raw data, and low quality reads (N content > 10%, more than 50% of bases with  
137 quality values < 10) were removed. Given the paucity of genomic resource for *H. annectans* and related  
138 species (e.g. Hylidae), we clustered all the paired-end reads into SLAF loci with clear index information  
139 based on sequence similarity above 90% using BLAT (Kent 2002) and concatenated all loci into a "fake"  
140 reference genome. For each locus the reference sequence was selected based on maximum sequencing  
141 depth of the corresponding SLAF tag. We used these matched sequences as our reference for sequence  
142 alignment and SNP calling. High-quality reads were mapped onto this reference using BWA-MEM (Li  
143 & Durbin 2009). The mapped reads were then sorted and duplicate reads were removed using PICARD-  
144 TOOLS v.1.67 (<http://broadinstitute.github.io/picard/>). Local realignment around the indel-regions was  
145 performed using RealignerTargetCreator and IndelRealigner in GATK (Genome Analysis Toolkit;  
146 McKenna *et al.* 2010). Since different variant calling pipelines may be prone to unique biases and  
147 provide inconsistent results (O'Rawe *et al.* 2013; Clevenger *et al.* 2015), we called variants using both  
148 the mpileup command in SAMTOOLS v.1.1 (Li *et al.* 2009) and GATK UnifiedGenotyper with default  
149 settings. We selected the concordant common sites identified by both GATK and SAMTOOLS using  
150 the SelectVariants package with default settings in GATK. Variant filtering was performed following  
151 the 'Best Practices' workflow developed by the GATK team (McKenna *et al.* 2010). Sequencing depths  
152 of each sample were calculated using the 'Depth of Coverage' module of GATK after removing indels  
153 with the SelectVariants package in GATK. The number of SLAF tags varied from 90,581 to 162,334  
154 across individual samples, and a total of 1,075,515 SLAF tags and 2,303,646 biallelic SNPs were  
155 retained. For phylogenetic and population genetic analyses, we excluded SNPs with allele count < 35

156 and with missing data over 20% across all individuals. Only one SNP per locus was retained. Individuals  
157 with more than 40% missing data were removed (Zhao *et al.* 2016). The final filtered dataset included  
158 8,420 informative SNPs. For divergence time estimation and TREEMIX analyses, only SNPs with  
159  $MAF > 0.05$  and with less than 5% or 10% missing data, respectively, were retained. For demographic  
160 analyses (i.e. STAIRWAY PLOTS) no missing data were allowed, and the data were not filtered for  
161  $MAF$  to avoid distorting the allele frequency spectra. More details on the different datasets are given in  
162 Supplementary Table S2.

### 163 **Phylogenetic inference**

164 A phylogeny of *H. annectans* populations was first estimated by constructing a Neighbor Joining (NJ)  
165 tree based on maximum composite likelihood with 10,000 bootstrap replicates using the MEGA X  
166 software (Kumar *et al.* 2018), with *H. sanchiangensis* as an outgroup. We estimated divergence times  
167 among lineages under the Multispecies Coalescent using the SNAPP v1.4.1 (Bryant *et al.* 2012) plugin  
168 of BEAST v2.4.4 (Bouckaert *et al.* 2014) with a molecular clock model (Stange *et al.* 2018). Since  
169 SNAPP is too computationally demanding to analyze all our individuals, we used a smaller dataset of  
170 72 individuals generated by randomly sampling two individuals from each site and from the outgroup.  
171 This dataset included a total of 2,183 SNPs with  $< 5\%$  missing data. We used the time to most recent  
172 common ancestor (tMRCA) of *H. annectans* (set as a lognormal distribution with  $4 \text{ Mya} \pm 0.14$ ) and  
173 tMRCA between *H. annectans* and the outgroup *H. sanchiangensis* (set as a lognormal distribution with  
174  $11.6 \text{ Mya} \pm 0.18$ ) as calibration nodes. We obtained these priors from a time-calibrated phylogeny of  
175 the genus *Hyla* based on mitochondrial and nuclear genetic data with three fossil calibration points (Li  
176 *et al.* 2015a). In SNAPP, we ran three independent analyses with 1,000,000 MCMC iterations. We  
177 thinned each chain by sampling every 1,000 trees to reduce serial correlation and checked the  
178 convergence of the MCMC and effective sample sizes (above 200) in TRACER v.1.7 (Rambaut *et al.*  
179 2018). We combined the results from the three independent chains in LOGCOMBINER v2.4.4  
180 (Bouckaert *et al.* 2014). We used the program DENSITREE v.2.2.6 (Bouckaert *et al.* 2014) to visualize

181 the SNAPP trees after discarding the first 10% of each MCMC chain as burn-in. Finally, we summarized  
182 the maximum-credibility trees with median heights in TREEANNOTATOR v.2.4.4 (Drummond &  
183 Rambaut 2007).

#### 184 **Molecular diversity and genetic structure**

185 We examined the patterns of genetic structuring among *H. annectans* populations with two different  
186 methods. Firstly, we used the fast variational Bayesian algorithm implemented in the software  
187 fastSTRUCTURE (Raj *et al.* 2014). Values for  $K = 2-15$  were tested to determine the optimal number  
188 of clusters ( $K$ ) using the Bayesian model selection criterion provided by fastSTRUCTURE. We ran the  
189 analyses for the best-supported number of clusters by *a*) using the *chooseK.py* program (Raj *et al.* 2014),  
190 which infers the best fitting model as the number of  $K$  that maximizes the marginal likelihood low bound  
191 (LLBO), and *b*) running a fivefold cross-validation and choosing the value of  $K$  that minimized  
192 prediction error. To visualize population structure, we used the web application POPHELPER (Francis  
193 2017). Secondly, we ran a principal component analysis (PCA) based on the sample covariance matrix  
194 of the SNP data (Patterson *et al.* 2006) using the R package ADEGENET (Jombart 2008).

195 After defining the genetic lineages of *H. annectans* on the basis of genetic clustering and phylogenetic  
196 analyses, we calculated genetic diversity indices including the expected ( $He$ ) and observed  
197 heterozygosity ( $Ho$ ) for each lineage using the R package ADEGENET (Jombart 2008). We estimated  
198 pairwise  $F_{ST}$  among genetic clusters in ARLEQUIN v.3.5.2.2 (Excoffier & Lischer 2010); 10,000  
199 permutations were run to test for statistical significance.

#### 200 **Importance of environmental and geographical factors in explaining genetic differentiation**

201 We plotted Slatkin's linearized  $F_{ST}$  (Slatkin 1995) against geographic distance to determine whether the  
202 observed patterns of genetic differentiation conform to Isolation by Distance model (IBD), and tested  
203 for a correlation between genetic and geographic distance matrices using a Mantel test with the ADE4

204 package in R. We estimated geographic distances calculated in ARCMAP implemented in ARCGIS  
205 Desktop version 10.3 (ESRI) based on latitude and longitude data for sampling site, and extracted the  
206 values using the “point distance” function.

207 In addition, we used a distance-based redundancy analysis (dbRDA) to test the effects of environmental  
208 and geographical factors on explaining genetic differentiation of *H. annectans* populations. We set the  
209 pairwise  $F_{ST}$  as response variable. To obtain geographic explanatory variables, we computed a Euclidian  
210 distance matrix from the Cartesian coordinates for each sampling site using the “dist” function and  
211 performed the “pcnm” function (permutations = 1000) on this matrix to obtain uncorrelated vectors. We  
212 then selected the positive eigenvectors as spatial variables as they were positively correlated with the  
213 geographic distance. The first three positive vectors (GEO1, GEO2, GEO3) were retained and used to  
214 run the dbRDA analysis. As environmental explanatory variables, we used four climatic variables  
215 (BIO1, BIO2, BIO12 and BIO14) that minimized collinearity. We estimated the relative contributions  
216 of both geographic and environmental variables and their intersection by variance partitioning. We  
217 additionally applied the dbRDA to detect IBD, considering the widespread concerns about the reliability  
218 of Mantel tests (Kierepka & Latch 2014). All those analyses were performed by the “capscale” and  
219 “anova.cca” functions in R package VEGAN (Oksanen *et al.* 2019).

## 220 **Demographic analyses**

221 We estimated past changes in effective population size ( $N_e$ ) for each sampling location with  
222 STAIRWAY PLOTS derived from folded SFS data (Liu & Fu 2015) in order to evaluate the effects of  
223 paleoclimatic changes. Since  $F_{ST}$  values were significant among most of the population pairs, we  
224 estimated the SFS for every single sampling location from a subset of biallelic SNPs with no missing  
225 data using ANGSD (Korneliussen *et al.* 2014), which resulted in 35 SNP datasets (Table S2). To  
226 construct STAIRWAY PLOTS, we used the default 2/3 of the data for training and [(nseq-2)/4, (nseq-  
227 2)/2, 3\*(nseq-2)/4 and (nseq-2)] as the number of random breakpoints (nrand, where nseq indicates the

228 number of sequences). We set generation time and mutation rate to two years (Liao & Lu 2010) and  
229  $1.552 \times 10^{-9}$  substitutions per site per generation (Sun *et al.* 2015), respectively.

230 We reconstructed migration events among *H. annectans* populations using TREEMIX v1.12 (Pickrell  
231 & Pritchard 2012) based on 2,118 informative SNPs. The model scenario was specified as follows: we  
232 set the number of migration events to be from 1 to 20 ( $m=1-20$ ), block size to 50, and *H. sanchiangensis*  
233 as the outgroup for the purpose of rooting. To evaluate the optimal number of migrations, we calculated  
234 the variance of relatedness between populations explained by the model using  
235 *TreemixVarianceExplained.R* (<https://github.com>), with over 99.8% of variance suggesting a reliable  
236 model (Pickrell & Pritchard 2012).

### 237 **Species distribution modelling (SDM)**

238 We generated SDMs for four time periods: the present time, the Mid-Holocene (5–7.5 kya), the Last  
239 Glacial Maximum (LGM; about 21 kya) and the Last Interglacial (LIG; about 120–140 kya) to  
240 investigate the possible influence of climatic changes on the distribution of *H. annectans*, using  
241 MAXENT v.3.3.3e (Phillips *et al.* 2006). We obtained the occurrence data of *H. annectans* used to build  
242 the SDMs in this study from four sources: samples used in this study, two literature records (Liao & Lu  
243 2010; Shen 1996), the Global Biodiversity Information Network GBIF (<http://www.gbif.org>), and  
244 VertNet (<http://vertnet.org/>; [Table S3](#)). Firstly, we removed data with no detailed locality information,  
245 imprecise GPS coordinates, obviously erroneous location (i.e. located in water bodies), as well as  
246 duplicate data. We only retained data at a resolution higher than 5 km, which corresponds to the  
247 resolution of the climatic data of each grid cell with size of 2.5 arc minutes (approximately 5 km). This  
248 resulted in a total 119 occurrence data points (Table S3). They were further assigned to main lineages  
249 (*viz.* lineage E [n=23], C [n=26], N1 [n=15], N2 [n =12], and W [n=43]) as inferred by the  
250 phylogeographic analyses (see Results). We searched for the best combinations of feature classes  
251 (determining the shape of the response curves) and regularization multipliers (determining the penalty

252 for adding parameters in the model) by evaluating model scores based on the Akaike information  
253 criterion (AICc). We used the ENMeval package (Muscarella *et al.* 2014) to identify the best model  
254 with the “ENMevaluate” function in R. The model feature types used were ‘L’, ‘H’, ‘LQ’, ‘LQH’, ‘LQHP’,  
255 ‘LQHTP’ (where: L = linear, Q = quadratic, H = hinge, P = product and T = threshold) and regularization  
256 (RM) values (0, 0.5, 1, 1.5, 2, 2.5, 3, 3.5, 4). For a proper evaluation, we calibrated SDMs using a  
257 random subset of 75% of the sampling sites; the remaining 25% were reserved to test the validity of the  
258 models. We used 19 bioclimatic layers as environmental predictors at 30-arcsec (~1 km) resolution,  
259 which we downloaded from the WorldClim database (<http://www.worldclim.org/>; Hijmans *et al.* 2005).  
260 To avoid multicollinearity, we selected BIO (bioclimatic variables) parameters using PCA. The results  
261 showed that the variance of the climate in the study area could be explained by four principal  
262 components (PCs) that captured 90% of the variance in the data. Thus, we selected one representative  
263 BIO parameter per PC (BIO1 = Annual Mean Temperature, BIO2 = Mean Diurnal Range, BIO12 =  
264 Annual Precipitation and BIO14 = Precipitation of Driest Month, Table S4) to create the SDMs. The  
265 three general circulation models (GCMs) used to generate Mid-Holocene and LGM climate scenarios  
266 were the CCSM4, MIROC-ESM (Watanabe *et al.* 2011) and MPI-ESM-P models available from the  
267 WorldClim database (<http://www.worldclim.org/>). Only one GCM of the LIG period was available. We  
268 used ARCGIS v.10.3 to manipulate and visualize the spatial environmental data and model output.

269 We employed the Mobility-oriented parity (MOP; Owens *et al.* 2013) analysis to assess if the study  
270 areas had similar environmental conditions currently, during the LGM and during the LIG, and if  
271 extrapolation risks exist. We used the 10% as a subsampling percentage for study area in the current  
272 climate. We performed the analysis using the KUENM package (Cobos *et al.* 2019) in R.

### 273 **Niche divergence**

274 We compared SDMs products for the five main lineages (E, C, N1, N2 and W) separately, to evaluate  
275 niche divergence in their predicted niche distribution by using ENMTools (Warren *et al.* 2008). We  
276 utilized two metrics for calculating niche divergence from the MAXENT: Schoener’s *D* (Schoener



277 1968) and Warren's *I* statistic (Warren *et al.* 2008). Both metrics range from 0 to 1, with 0 corresponding  
278 to identical niches and 1 representing no niche divergence between the two compared groups.

### 279 **Morphological analyses**

280 We also tested for differences between the main identified lineages and/or recognized subspecies (Fei  
281 *et al.* 2009). For each collected individual, we counted the number of distinct round black spots on the  
282 right (posterior) side of the body, as this is a taxonomically diagnostic character used to demarcate  
283 different subspecies (Fei *et al.* 2009). We measured the snout-vent length (SVL) to the nearest 0.01 mm  
284 with digital calipers and weighed the specimens to the nearest 0.1g with electronic digital balance. In  
285 total, we grouped 339 individuals (10 individuals from population "2" were not measured) according to  
286 their genetic cluster and compared the mean values of black spot numbers across clusters using a  
287 Kruskal-Wallis test, as trait values were not normally distributed. We also compared mean size and  
288 weight of individuals using a parametric ANOVA, as these traits were normally distributed. We  
289 performed all statistical using the SPSS software (SPSS 22.0, SPSS Inc, Chicago, IL, USA) and tested  
290 for significance at an alpha level of 0.05. We visualized the relationship between the number of black  
291 spots and the seven genetic clusters in R v.3.2.2 (R Core Team 2014).

### 292 **$Q_{ST}$ - $F_{ST}$ comparison**

293 We conducted  $Q_{ST}$ - $F_{ST}$  comparisons to explore whether the degree of phenotypic differentiation in three  
294 traits (number of spots, snout-vent length, and weight) exceeded neutral expectation – which would  
295 indicate differentiation driven by natural selection – by using the R packages RAFM and DRIFTSEL  
296 (Ovaskainen *et al.* 2011; Karhunen *et al.* 2013). A  $Q_{ST}$  is a metric equivalent to  $F_{ST}$  – while the latter is  
297 estimated from genetic marker data and reflects the degree of neutral genetic differentiation, the former  
298 is derived from phenotypic data reflects the degree of differentiation in quantitative traits (e.g. Leinonen  
299 *et al.* 2013). A  $Q_{ST}$  significantly larger than  $F_{ST}$  would be indicative of differentiation in given  
300 quantitative trait exceeding neutral expectation, and hence, that the divergence in trait values is driven

301 by natural selection (Leinonen *et al.* 2013). Compared to conventional frequentist approaches, the  
302 RAFM/DRIFTSEL uses MCMC-based Bayesian algorithms to account for patterns of relatedness  
303 among populations, as well as ancestral genetic correlations among the traits of interest, hence the power  
304 to detect signatures of selection from data with small sample sizes is stronger than the conventional  $Q_{ST}$ -  
305  $F_{ST}$  comparisons (Ovaskainen *et al.* 2011). First, the RAFM software calculated the  $F_{ST}$  and the genomic  
306 relatedness among the 35 populations based on the 8,420 SNPs. Next, we used DRIFTSEL to estimate  
307 the  $Q_{ST}$  of the three traits: number of black spots, snout-vent length and weight, and also to perform the  
308 comparison between  $Q_{ST}$  and  $F_{ST}$ . The final output of the DRIFTSEL analysis is a so-called S-statistic.  
309 S-values close to zero are indicative of stabilizing selection; those close to one indicate directional  
310 selection; and values close to 0.5 are consistent with evolution due to drift. Following the testing criteria  
311 proposed in Karhunen *et al.* (2014),  $S > 0.95$  implies that a quantitative trait has evolved under divergent  
312 selection at the 95% credibility level, whereas  $S < 0.05$  would imply stabilizing selection at the same  
313 credibility level. The default non-informative priors were used in the DRIFTSEL analyses. 15,000  
314 Markov Chain Monte Carlo (MCMC) samples of the posterior distribution were simulated, and the first  
315 5,000 were discarded as burn-ins. The remaining were stored in every 10th iteration, so that eventually  
316 1,000 MCMC samples were used for calculating S-statistics.

317 We estimated the added variance component for the three abovementioned phenotypic traits to see  
318 whether the degree of phenotypic divergence is predictable from the degree of genetic divergence ( $F_{ST}$ ),  
319 using a standard ANOVA approach (Sokal and Rohlf 1981). This quantity named as  $P_{ST}$  (Leinonen *et*  
320 *al.* 2013) is similar to  $Q_{ST}$  (= the degree of genetic differentiation in quantitative traits; Leinonen *et al.*  
321 2013) under certain assumptions (within- and among-population components of variance are not  
322 confounded by environmental effects; Brommer 2011; Leinonen *et al.* 2013, see also Discussion). Since  
323 there is no reason to assume that these quantities would be normally distributed, we used Spearman rank  
324 correlation coefficient for testing this association.

## 325 **Results**

## 326 **Sequencing and SNP calling**

327 We sequenced 349 individuals of *H. annectans* using an Illumina HiSeq<sup>TM</sup>2500, generating a total of  
328 479 million paired-end reads. There were 82.78% bases with quality scores of at least 30 (Q30) and the  
329 guanine-cytosine content was 42.06%. We obtained 1,075,515 tags (or SLAFs) in total, and their  
330 average sequencing depth was 5.53 (Table S5). A total of 2,303,646 bi-allelic SNPs were obtained. After  
331 filtering, the four datasets contained 8,420 SNPs for phylogeny and structure analysis, 2,118 for  
332 estimating gene flow, 2,183 for divergence time estimation, and 3,002–14,842 SNPs (depending on the  
333 population) for analyses of historical demography.

## 334 **Phylogenetic inference**

335 Phylogenetic analyses based on 8,420 SNPs revealed seven major genetic clusters in the NJ-tree,  
336 concordant with geography (Figure 1). The eastern cluster (E) included 11 populations from the Wuling  
337 Mountains (Figure 1). The central cluster (C), which contained two sub-clusters (C1 and C2), included  
338 seven populations distributed across central and eastern Yunnan-Guizhou Plateau (Figure 1). The  
339 northern cluster (N) had two sub-clusters (N1 and N2), representing populations located in the Hengduan  
340 Mountains on the margin of the Sichuan Basin (Figure 1). The western cluster also contained two sub-  
341 clusters (W1 and W2) distributed along the Hengduan Mountains and western Yunnan-Guizhou Plateau,  
342 respectively (Figure 1).

343 We estimated that the lineages of *H. annectans* initiated their divergence during the Pliocene. The  
344 northern clade (N1 and N2) diverged from the other clades ca. 5.23 million years ago (Mya, with 95%  
345 highest posterior density interval (HDPI) of 4.38–6.55 Mya, Figure 2 and Figure S1). The eastern clade  
346 (E) diverged from the western and central clades (W and C) approximately 4.88 Mya (95% HDPI: 4.09–  
347 6.15 Mya). Lineages N1 and N2 diverged approximately 4.44 Mya (95% HDPI: 3.60–5.80 Mya) and  
348 subsequently, the western and central clades split into two clades at about 3.77 Mya (95% HDPI: 3.22–  
349 4.84 Mya). The genetic divergences within western and central clades were estimated to have occurred

350 at 2.32 Mya (95% HDPI: 1.63–2.90 Mya) for C1 and C2, and at 2.39 Mya (95% HDPI: 1.94–3.10 Mya)  
351 for W1 and W2 (Figure 2 and Figure S1).

## 352 **Molecular diversity and genetic structure**

353 The variation in observed and expected heterozygosity among clusters was considerable, ranging from  
354 0.013 (population 22) to 0.134 (population 11) for observed heterozygosity, and from 0.014 (population  
355 22) to 0.177 (population 11; Table S6) for expected heterozygosity. The highest observed and expected  
356 heterozygosities occurred in clusters E, C1 and C2, which were located in the Wuling Mountains and  
357 the East Yunnan-Guizhou Plateau (Table S6). Pairwise  $F_{ST}$  values were all statistically significant, with  
358 an average pairwise  $F_{ST} = 0.669$ , ranging from 0.016 to 0.957 ( $P < 0.001$ ; Table S6), suggesting that *H.*  
359 *annectans* populations are geographically highly structured.

360 The Bayesian clustering algorithm implemented in fastSTRUCTURE detected a clear geographical  
361 pattern of subdivision (optimal  $K = 7$ , Figures 3a and S2). At  $K = 2$ , the eastern (E) cluster was distinct  
362 from other clusters (Figure 3a); at  $K = 3$ , the western clusters (W1 and W2) were distinct from the central  
363 (C1 and C2) and northern (N1 and N2) clusters; at  $K = 4$ , the central clusters separated from the northern  
364 clusters; at  $K = 5$ , the northern clusters were divided into N1 and N2; at  $K = 6$ , the central cluster was  
365 divided into two sub-clusters C1 and C2, where population 15 was an admixture between the two sub-  
366 clusters; at  $K = 7$ , the W2 cluster showed signs of admixture with an unsampled population. In addition,  
367 within the western cluster, cluster W2 was indicated to be an admixture between western and central  
368 clusters at  $K = 3-6$ ; three populations ('9', '10' and '11') from the eastern cluster showed signs of  
369 admixture with the central cluster (C1) at  $K = 2-7$ . The clustering analyses using the simple models  
370 showed an optimal choice of  $K = 7$ , which had the lowest value of cross-validation (CV) error and the  
371 highest marginal likelihood (Figure S2). While the W1 and W2 clusters were adjacent, they were clearly  
372 separated in the PCA. Similarly, while the geographic distance separating clusters N1 and N2 was very  
373 short (e.g. the distance between sampling locations '20' and '22' is 38 km), all analyses indicated that

374 they were very highly differentiated ( $F_{ST} = 0.956$ ) independent genetic clusters. In summary, results  
375 from the fastSTRUCTURE, PCA, and phylogenetic analyses suggest that the 35 *H. annectans*  
376 populations sampled from southwestern China are divided into seven geographically and genetically  
377 distinct lineages (N1, N2, W1, W2, C1, C2 and E).

### 378 **Importance of environmental and geographical factors in explaining genetic differentiation**

379 The IBD test revealed a weak but significant correlation (dbRDA  $r^2_{adj} = 0.171$ ,  $P = 0.001$ ; Mantel test  
380 statistic  $r^2 = 0.015$ ,  $P = 0.003$ ; Figure S3) when all populations were included. However, a few  
381 populations deviating from the general pattern (populations in clusters N1, N2 and W1 located at  
382 opposite sides of the Hengduan Mountains) showed a very high degree of differentiation over short  
383 geographic distances, suggesting very limited gene flow despite close geographic proximity. When we  
384 excluded these deviating populations, which comprised 14 out of the 35 sampling locations, a much  
385 stronger IBD was apparent (dbRDA  $r^2_{adj} = 0.454$ ,  $P = 0.001$ ; Mantel test statistic  $r^2 = 0.343$ ,  $P < 0.001$ ;  
386 Figure S3).

387 The redundancy analyses revealed that the contribution of environmental variables to genetic divergence  
388 was somewhat higher than that of geographic variables (41 and 37%, respectively; Table 1). The  
389 variance partitioning test showed that the environmental and geographic variables explained 15.1% and  
390 14.7% of the variance, respectively, whereas their intersection explained 7% of variance (Figure S4).

### 391 **Demographic analyses**

392 The STAIRWAY PLOTS revealed diverse demographic histories for populations from different  
393 lineages. Populations in lineages W1, W2, E, C1 and C2 maintained stable population sizes during the  
394 LIG (Figure 4). Most of the populations within the Eastern and Central clusters experienced a moderate  
395 population size contraction during or shortly after the LGM or the Holocene Optimum. Populations

396 within clusters N1, N2 and W1 showed clear signs of strong population contractions followed by  
397 expansions during the Holocene Optimum and the LGM, respectively (Figure 4a,b,c).

398 Although populations in the seven genetic lineages diverged and experienced different demographic  
399 histories, TREEMIX analyses (99.8% of variance explained) identified 12 migration events between  
400 populations (Figure 4h). Specifically, obvious migration events from populations in lineage C1 to the  
401 populations in lineage E, and between populations in C groups with populations in lineage W2 (Figure  
402 4h). We also found two weakly supported migration events from populations in lineage W2 to  
403 populations in lineage N2, and the ancestor of the northern populations could be attributed to an  
404 admixture event with the W2 lineages. Interestingly, there was a clear migration event from lineage E  
405 to lineage N1 despite the long geographic distance separating them, whereas no distinct migration event  
406 was detected between populations in lineages N1 and N2, which are closest together (Figure 4h).

#### 407 **Species distribution modelling**

408 The lowest AICc was assigned to the LQHP 1 model (Figure S5 and Table S7), and this was chosen to  
409 generate the projections of species distribution model. The distribution model accurately predicted the  
410 distribution area under the curve (AUC) values (mean  $\pm$ SE: 0.951  $\pm$ 0.123, Table S8), indicating a good  
411 performance of the predictive models. The predicted current species distribution area was generally  
412 similar to the actual known distribution area in China (Figure 1, 6 and Figure S6). The overall suitable  
413 distribution areas of all lineages shrank gradually from the LIG to LGM (Figure 5 and Figure S6). The  
414 suitable distribution areas of the N1 lineage was indicated to have reduced significantly, especially for  
415 the northwest corner of the Sichuan Basin from the LGM to the present (Figure 5c and Figure S6). The  
416 suitable distribution area of the N2 lineage was indicated to have shrank in the south region from the  
417 LGM to the present (Figure 5d and Figure S6). In contrast, several other regions including the southern  
418 Hengduan Mountains (sites for lineage W; Figure 5e and Figure S6), Yunnan-Guizhou Plateau (sites for

419 lineage C; Figure 5b and Figure S6) and Wuling Mountains (sites for lineage E; Figure 5a and Figure  
420 S6) have reduced slightly in size from the LGM to the present.

421 The MOP analyses demonstrated that past scenarios mostly possess climates analogous to those in the  
422 current scenario in the distribution areas of *H. annectans* (Figure S7). Most of the strict extrapolation  
423 risk was present in the northern and eastern parts of the distribution maps for each period (HM, LGM,  
424 and LIG; Figure S7).

#### 425 **Niche divergence**

426 Based on both Schoener's *D* and Warren's *I*, there was stronger niche divergence between the  
427 comparisons involving C and N1 lineages, E and N1 lineages, E and N2 lineages, E and W lineages than  
428 in the comparisons of between the N1 and W lineages, W and C lineages, and E and C lineages (Table  
429 2). It is notable that the comparison of the geographically closely located N1 and N2 lineages, a moderate  
430 degree niche divergence was observed (Schoener's *D* = 0.337; Warren's *I* = 0.634, Table 2).

#### 431 **Morphological variation**

432 Comparison of mean number of black spots among the seven genetic clusters revealed significant  
433 differences between the clusters (Table 3). Comparisons of mean snout-vent length and weight among  
434 the genetic clusters also indicated significant differences (ANOVAs, snout-vent length:  $F_{6,319} = 3.13$ ,  $P$   
435  $< 0.01$ ; Weight:  $F_{6,319} = 9.96$ ,  $P < 0.01$ ). However, only few pairwise comparisons revealed significant  
436 differences in SVL (4.67% of comparisons) and weight (33.3% of comparisons; Table S9).

#### 437 **$Q_{ST}$ - $F_{ST}$ comparison**

438 DRIFTSEL yielded  $S = 0.95$  for number of black spots, 0.44 for snout-vent length, 0.45 for weight and  
439 0.84 for all three traits tested together. Hence, the only evidence for natural selection was differentiation  
440 in the number of black spots, but not for the other traits whether considered separately or together.

441 Likewise, the correlations between pairwise  $F_{ST}$  and pairwise  $P_{ST}$  for the three different phenotypic traits  
442 were significant for number of black spots ( $r_{337} = -0.53$ ,  $P = 10^{-16}$ ), but not for snout-vent length ( $r_{337} =$   
443  $-0.18$ ) or weight ( $r_{337} = -0.09$ ).

## 444 **Discussion**

445 We discovered that *H. annectans* in southern China consists of seven phylogenetic lineages with  
446 parapatric distributions. These lineages show high levels of genetic differentiation and also clear  
447 phenotypic divergence likely attributable to natural selection. These distinct genetic lineages diverged  
448 from each other 2.32 to 5.23 Mya, a timing that is broadly consistent with the rapid and intense uplift of  
449 the QTP and adjacent southwest China (Cui *et al.* 1996; Sun *et al.* 2011). The results further indicate  
450 that both geographic and environmental factors have contributed to the observed genetic differentiation.  
451 Demographic analyses and SDMs demonstrated that Pleistocene climatic fluctuations had different  
452 impacts on both population sizes and the extent of suitable habitat of different populations, possibly  
453 reflecting the fact that the past climatic conditions in the Hengduan Mountains differed from those in  
454 southern China. In the following, we will discuss these findings in more detail.

455 At range-wide level, seven deeply divergent genetic lineages with parapatric distributions were  
456 discernable with phylogenetic, ordination and Bayesian clustering approaches. Although, we could have  
457 split W1 cluster into two further clusters from the PCA and the SNAPP tree, it would not have  
458 profoundly altered the results. These two sampling locations include only 20 individuals, which is  
459 roughly 5.7% of the data. The deep genetic divergence among different *H. annectans* lineages may be  
460 explained by two non-mutually exclusive biotic factors. First, it may be attributable to the limited  
461 dispersal capability of *H. annectans*. Geographic distance explained 23% of the variance in genetic  
462 differentiation, and a clear and strong pattern of isolation-by-distance was observed across most of the  
463 study populations. Second, the strong genetic structuring could be a result of the species-specific habitat  
464 requirements. The occurrence of *H. annectans* in China is restricted to mountain forests in low-to-



465 medium elevations (Fei *et al.* 2009), which suggests that dispersal over high elevation mountain ranges  
466 is unlikely (see Figure 1). Consistent with this hypothesis, we found that elevation explained over 14%  
467 of genetic differentiation of *H. annectans*.

468 We estimated that the seven genetic lineages of *H. annectans* diverged in the Pliocene (2.32–5.23 Mya).  
469 This timing matches the rapid and intense uplift of the QTP and adjacent Southwest China: the oldest  
470 uplifting starting about 8 Mya (Harrison *et al.* 1992) and was followed by several mid-Pliocene events  
471 (Cui *et al.* 1996; Sun *et al.* 2011). Each phase of these geological movements likely generated barriers  
472 to gene flow leading to strong genetic differentiation among populations and lineages in the southern  
473 mountains of China. For instance, the inferred divergence time of the N1 and N2 lineages at 4.4 Mya  
474 implicates the rise of Daxiangling Mountains as a probable driver of divergence. The intense uplifting  
475 of the mountain range in the western Sichuan basin, including the Daxiangling Mountains, occurred  
476 after the Miocene and reached peak elevation shortly before the Late Pliocene (Sun *et al.* 2011).  
477 Similarly, lineages W and N located in the opposite sides of the Hengduan Mountains likely diverged  
478 as a direct consequence of the uplift of the Hengduan Mountains, including Shaluli Mountains and  
479 Daxue Mountains located in this area. Further evidence for strongly restricted gene flow across the  
480 Hengduan Mountains was provided by our isolation-by-distance (IBD) analyses. We found that the  
481 pattern of IBD was weak (albeit statistically significant) when considering all populations, but became  
482 much stronger after removing populations from the high altitude lineages (W1, N1 and N2) located at  
483 opposite sides of the Hengduan Mountains. Similar uplift-driven diversification in southern China have  
484 also been reported from earlier studies of plants (Xing & Ree 2017) and animals (Yan *et al.* 2013; Li *et*  
485 *al.* 2015b). Thus, the complex geological events leading to habitat fragmentation and barriers to gene  
486 flow appear to be responsible for the high levels of intra- and interspecific diversity in the southern  
487 mountains of China.

488 Pleistocene climatic fluctuations have had strong influence on demographic processes and distribution  
489 of taxa in Europe and North America (Hewitt 2000; Hewitt 2004). In southern China, the role of

490 paleoclimatic fluctuations on demographic processes and distribution of taxa have remained  
491 controversial. Some studies have reported that Pleistocene climatic oscillations have shaped current  
492 patterns of genetic variation in various taxa (Ye *et al.* 2014; Li *et al.* 2018), whereas other studies have  
493 produced contradictory evidence (Wang & Ge 2006; Gao *et al.* 2011; Yan *et al.* 2013). One possible  
494 reason for these opposing results could be methodological: estimation of demographic history with  
495 limited genetic data may lead to biased inferences (Avice 2000; Ballard & Whitlock 2004; Guo *et al.*  
496 2019). Here we were able to accurately reconstruct temporal changes in effective population size of the  
497 different lineages: these results suggest a heterogeneous effect of paleoclimatic factors on the  
498 demographic history of different *H. annectans* lineages. We found fluctuations in historical effective  
499 population sizes that followed Pleistocene climatic cycles, as well as changes in the extent and  
500 distribution of potential habitat for this species from the LIG to the present. These patterns highlight this  
501 species' sensitivity to temperature changes, in accordance with our findings that two climatic factors  
502 (BIO1 and BIO2) were strong predictors of the degree of genetic differentiation among different  
503 lineages.

504 The species' response to paleoclimatic changes was geographically heterogeneous. Populations  
505 distributed around the Hengduan Mountains (lineages N1, N2 and W1), displayed an obvious bottleneck  
506 following the LGM or Mid-Holocene, and had the lowest heterozygosities of all studied populations.  
507 The results from species distribution models suggest that the N1 lineage experienced severe range  
508 contraction and that the southern distribution of the N2 lineage shrank from LGM to present. Such  
509 pattern is compatible with two indistinguishable demographic scenarios: the invasion of a completely  
510 novel habitat following the retreat of an ice sheet or extinction/re-colonization. In contrast, most of the  
511 populations from lineages W2, E, C1 and C2 experienced moderate and gradual declines following the  
512 LGM or Mid-Holocene, as well as slight range contradictions (Figure 5). Such incongruence in the past  
513 demographic histories of different lineages possibly reflects differences in habitat availability.  
514 Populations in the Hengduan Mountains occupy a relatively smaller effective habitat area (Figure 1)  
515 making them more sensitive to environmental changes in their geographic range as smaller populations

516 have higher risk of decline or extinction (Green 2003). This was particularly relevant during the LGM  
517 – the period with dry conditions, low temperatures and extended ice sheets (Gasse 2000; Clark *et al.*  
518 2009). The fastSTRUCTURE and TREEMIX analyses identified admixture events between the C and  
519 E, as well as the C and W2 lineages, which could be the result of homogeneous environmental condition  
520 in the Yunnan-Guizhou Plateau and Wuling Mountains. Gene flow likely increased genetic variation  
521 within these lineages, as these lineages show the highest observed and expected heterozygosities. On  
522 the other hand, low levels of contemporary and historical gene flow divergence between C with N1 and  
523 N2 lineages, in spite of geographical proximity, were associated with moderate ecological niche  
524 divergence between the C and the N1 and N2 lineages (Schoener's  $D = 0.230, 0.377$  and Warren's  $I =$   
525  $0.511, 0.653$ , respectively, Table 2).

526 A clear and strong IBD was observed across most of the study populations, suggesting that there is – or  
527 has been – some degree of gene flow between different lineages; this conclusion was also supported by  
528 the TREEMIX results. However, the N1 and N2 lineages were an exception. These are the two lineages  
529 that are geographically closest (38 km), and yet displayed extremely high genetic divergence ( $F_{ST} =$   
530  $0.909$ ), suggesting the absence of gene flow. Such divergence is likely the result of geological barriers  
531 (in this case: Daxiangling Mountains) and strong genetic drift. Interestingly, these lineages also showed  
532 moderate niche divergence (Schoener's  $D = 0.337$  and Warren's  $I = 0.634$ ), suggesting that they may be  
533 also ecologically divergent. However, the current distribution range of the N1 lineage may not reflect  
534 its past distribution. As shown by the SDM results, the habitat suitable for the N1 lineage around the  
535 northwest corner of Sichuan Basin contracted gradually from the LIG to the present. This interpretation  
536 is also supported by the observation that the populations in the N1 and N2 lineages were found to have  
537 experienced population size bottlenecks at different time periods.

538 Apart from the deep genetic divergences revealed by both phylogenetic analyses and high pairwise  $F_{ST}$   
539 values, the seven major lineages exhibited clear differentiation in phenotypic traits. Although  
540 differentiation in the mean values of all studies traits was significant, DRIFTSEL analyses suggest that

541 only divergence in the number of black spots was likely driven by selection. Since the data utilized in  
542 these analyses came from wild-collected individuals, rather than from a common garden experiment,  
543 the results should be interpreted with caution (Karhunen *et al.* 2013; Leinonen *et al.* 2013). Namely, the  
544 possibility of environmentally induced differences cannot be excluded as an alternative explanation for  
545 divergence in the number of black spots. Regardless of whether this divergence was genetic,  
546 environmental, or due to their combined effects, it is noteworthy that the magnitude of phenotypic  
547 differentiation ( $P_{ST}$ ) exceeded, on average, that of neutral genetic differentiation ( $F_{ST}$ ). Since the neutral  
548 expectation is that  $P_{ST} \approx F_{ST}$ , any deviation from this calls for an explanation. Similarly, the fact that  
549 phenotypic differentiation was a negative function of neutral differentiation is noteworthy. The  
550 mechanistic explanation for this negative correlation is that some of the most genetically divergent  
551 populations were phenotypically the least diverged (e.g. lineages N1, N2 and E in Figure 2). Without  
552 common garden data, we cannot conclusively establish an ultimate explanation for the observed  
553 patterns. Nevertheless, we suspect that the divergence in number of black spots may be related to  
554 different sexual selection regimes in different lineages, as observed in other systems (Endler 1983;  
555 Reynolds & Fitzpatrick 2007; Rudh *et al.* 2007). Hence, an interesting avenue for future studies would  
556 be to investigate whether the phenotypic differentiation in number of black spots might act as pre-  
557 zygotic isolation mechanism between the seven genetically divergent lineages.

## 558 **Conclusions**

559 In conclusion, our genome-wide analyses of *H. annectans* revealed seven highly differentiated genetic  
560 lineages, which also show clear phenotypic differences likely attributable to the action of natural  
561 selection. The estimated divergence times for these lineages closely align with the timing of the uplifting  
562 of the QTP and adjacent southwest China, suggesting that past geological events played a major role in  
563 shaping the distribution of genetic diversity within this species complex. Populations living in different  
564 areas displayed different demographic dynamics in response to Pleistocene and Holocene climatic  
565 changes. This is expected, because of the geographic and temporal variation in the climatic conditions  
566 experienced in different areas. As such, this study provides an example of how the combined effects of

567 geomorphological and climatic factors have shaped the distribution of genetic variation in a widely  
568 distributed species. The results highlight how geological events and topographic features play  
569 predominant roles as drivers of lineage differentiation, and that climatic fluctuations contribute to re-  
570 shaping the distribution of genetic variability.

## 571 **Acknowledgments**

572 We thank Chengliang Li, Wanxin Du, Jibing Liu, Youming Zhang and Xiaoran Zhu help with sample  
573 collection. Xueyun Feng and Bohao Fang kindly helped with solving analytical problems. We thank  
574 Jacquelin De Faveri for a linguistic check on an earlier version of this manuscript. We are also thankful  
575 for the computing resource support from CSC - the Finnish IT Center for Science Ltd administered by  
576 the Ministry of Education and Culture, Finland. Our research was supported by grants from the  
577 Biodiversity Survey, Monitoring and Assessment Project of Ministry of ecology and environment,  
578 China (2019–2023) and Academy of Finland (No. 129662, 134728 and 218343 to Juha Merilä and No.  
579 316294 to Paolo Momigliano).

## 580 **References**

- 581 Avise JC, Arnold J, Ball RM *et al.* (1987) Intraspecific phylogeography: the mitochondrial DNA bridge  
582 between population genetics and systematics. *Annual Review of Ecology and Systematics*, **18**,  
583 489-522.
- 584 Avise JC (1994) *Molecular Markers, Natural History and Evolution*. Chapman & Hall, New York.
- 585 Avise JC (2000) *Phylogeography: The History and Formation of Species*. Harvard University Press,  
586 Cambridge, Massachusetts.
- 587 Avise JC (2009) Phylogeography: retrospect and prospect. *Journal of Biogeography*, **36**, 3-15.
- 588 Ballard JW, Whitlock MC (2004) The incomplete natural history of mitochondria. *Molecular Ecology*,  
589 **13**, 729-744.
- 590 Bossuyt F, Milinkovitch MC (2001) Amphibians as indicators of early tertiary "out-of-India" dispersal  
591 of vertebrates. *Science*, **292**, 93-95.
- 592 Bouckaert R, Heled J, Kühnert D *et al.* (2014) BEAST 2: a software platform for Bayesian evolutionary  
593 analysis. *PLoS Computational Biology*, **10**, e1003537.
- 594 Brommer JE (2011) Whither  $P_{ST}$ ? The approximation of  $Q_{ST}$  by  $P_{ST}$  in evolutionary and conservation  
595 biology. *Journal of Evolutionary Biology*, **24**, 1160-1168.
- 596 Bryant D, Bouckaert R, Felsenstein J, Rosenberg NA, RoyChoudhury A (2012) Inferring species trees  
597 directly from biallelic genetic markers: bypassing gene trees in a full coalescent analysis.  
598 *Molecular Biology and Evolution*, **29**, 1917-1932.
- 599 Chaves JA, Weir JT, Smith TB (2011) Diversification in *Adelomyia* hummingbirds follows Andean  
600 uplift. *Molecular Ecology*, **20**, 4564-4576.
- 601 Che J, Zhou WW, Hu JS *et al.* (2010) Spiny frogs (Paini) illuminate the history of the Himalayan region  
602 and Southeast Asia. *Proceedings of the National Academy of Sciences USA*, **107**, 13765-13770.
- 603 Clark PU, Dyke AS, Shakun JD *et al.* (2009) The last glacial maximum. *Science*, **325**, 710-714.
- 604 Clevenger J, Chavarro C, Pearl SA, Ozias-Akins P, Jackson SA (2015) Single nucleotide polymorphism  
605 identification in polyploids: a review, example, and recommendations. *Molecular Plant*, **8**, 831-  
606 846.
- 607 Cobos ME, Peterson AT, Barve N *et al.* (2019) kuenm: an R package for detailed development of  
608 ecological niche models using Maxent. *PeerJ*, **7**, e6281.
- 609 Cui ZJ, Gao QZ, Liu GN *et al.* (1996) Planation surfaces, palaeokarst and uplift of Xizang (Tibet)  
610 Plateau. *Science in China Series D: Earth Sciences*, **39**, 391-400.

611 Drummond AJ, Rambaut A (2007) BEAST: Bayesian evolutionary analysis by sampling trees. *BMC*  
612 *Evolutionary Biology*, **7**, 214.

613 Dufresnes C, Strachinis I, Suriadna N *et al.* (2019) Phylogeography of a cryptic speciation continuum  
614 in Eurasian spadefoot toads (*Pelobates*). *Molecular Ecology*, **28**, 3257-3270.

615 Endler JA (1983) Natural and sexual selection on color patterns in poeciliid fishes. *Environmental*  
616 *Biology of Fishes*, **9**, 173-190.

617 Excoffier L, Lischer HE (2010) Arlequin suite ver 3.5: a new series of programs to perform population  
618 genetics analyses under Linux and Windows. *Molecular Ecology Resources*, **10**, 564-567.

619 Fei L, Hu SQ, Ye CY *et al.* (2009) *Fauna Sinica, Amphibia: Vol 2. Anura, Hylidae*. Science Press,  
620 Beijing.

621 Feng SH, Fang Q, Barnett R *et al.* (2019) The genomic footprints of the fall and recovery of the crested  
622 ibis. *Current Biology*, **29**, 340-349.

623 Francis RM (2017) Pophelper: An R package and web app to analyse and visualize population structure.  
624 *Molecular Ecology Resources*, **17**, 27-32.

625 Gao B, Yu LJ, Qu YH *et al.* (2011) An unstructured phylogeographic pattern with extensive gene flow  
626 in an endemic bird of South China: Collared finchbill (*Spizixos semitorques*). *International*  
627 *Journal of Molecular Sciences*, **12**, 3635-3647.

628 Gasse F (2000) Hydrological changes in the African tropics since the Last Glacial Maximum.  
629 *Quaternary Science Reviews*, **19**, 189-211.

630 Graham CH, Ron SR, Santos JC, Schneider CJ, Moritz C (2004) Integrating phylogenetics and  
631 environmental niche models to explore speciation mechanisms in dendrobatid frogs. *Evolution*,  
632 **58**, 1781-1793.

633 Green DM (2003) The ecology of extinction: population fluctuation and decline in amphibians.  
634 *Biological Conservation*, **111**, 331-343.

635 Guo BC, Fang BH, Shikano T, Momigliano P, Wang C, Kravchenko A, Meril äJ (2019) A phylogenomic  
636 perspective on diversity, hybridization and evolutionary affinities in the stickleback genus  
637 *Pungitius*. *Molecular Ecology*, **28**, 4046-4064.

638 Hanania U, Velcheva M, Sahar N, Perl A (2004) An improved method for isolating high-quality DNA  
639 from *Vitis vinifera* nuclei. *Plant Molecular Biology Reporter*, **22**, 173-177.

640 Harrison TM, Copeland P, Kidd WS, Yin A (1992) Raising Tibet. *Science*, **255**, 1663-1670.

641 Hewitt GM (1996) Some genetic consequences of ice ages, and their role in divergence and speciation.  
642 *Biological Journal of the Linnean Society*, **58**, 247-276.

643 Hewitt GM (2000) The genetic legacy of the Quaternary ice ages. *Nature*, **405**, 907-913.

644 Hewitt GM (2004) Genetic consequences of climatic oscillations in the Quaternary. *Philosophical*  
645 *Transactions of the Royal Society of London B: Biological Sciences*, **359**, 183-195.

646 Hijmans RJ, Cameron SE, Parra JL, Jones PG, Jarvis A (2005) Very high resolution interpolated climate  
647 surfaces for global land areas. *International Journal of Climatology*, **25**, 1965-1978.

648 Jiang WS, Qiu Y, Pan XF *et al.* (2018) Genome assembly for a Yunnan-Guizhou Plateau “3E” fish,  
649 *Anabarilius grahami* (Regan), and its evolutionary and genetic applications. *Frontiers in*  
650 *Genetics*, **9**, 614.

651 Jombart T (2008) adegenet: a R package for the multivariate analysis of genetic markers. *Bioinformatics*,  
652 **24**, 1403-1405.

653 Ju LX, Wang HJ, Jiang DB (2007) Simulation of the Last Glacial Maximum climate over East Asia  
654 with a regional climate model nested in a general circulation model. *Palaeogeography,*  
655 *Palaeoclimatology, Palaeoecology*, **248**, 376-390.

656 Karhunen M, Meril äJ, Leinonen T *et al.* (2013) Driftsel: an R package for detecting signals of natural  
657 selection in quantitative traits. *Molecular Ecology Resources*, **13**, 746-754.

658 Karhunen M, Ovaskainen O, Herczeg G *et al.* (2014) Bringing habitat information into statistical tests  
659 of local adaptation in quantitative traits: A case study of nine-spined sticklebacks. *Evolution*,  
660 **68**, 559-568.

661 Kent WJ (2002) BLAT-the BLAST-like alignment tool. *Genome Research*, **12**, 656-664.

662 Kierepka EM, Latch EK (2014) Performance of partial statistics in individual-based landscape genetics.  
663 *Molecular Ecology Resources*, **15**, 512-525.

- 664 Korneliussen TS, Albrechtsen A, Nielsen R (2014) ANGSD: analysis of next generation sequencing  
665 data. *BMC Bioinformatics*, **15**, 356.
- 666 Kozak KH, Wiens JJ (2010) Niche conservatism drives elevational diversity patterns in Appalachian  
667 salamanders. *American Naturalist*, **176**, 40-54.
- 668 Kumar R, Kumar V (2018) A review of phylogeography: biotic and abiotic factors. *Geology, Ecology,  
669 and Landscapes*, **2**, 268-274.
- 670 Kumar S, Stecher G, Li M *et al.* (2018) MEGA X: Molecular evolutionary genetics analysis across  
671 computing platforms. *Molecular Biology and Evolution*, **35**, 1547-1549.
- 672 Leinonen T, Scott McCairns RJ, O'Hara RB, Merilä J (2013)  $Q_{ST}$ - $F_{ST}$  comparisons: evolutionary and  
673 ecological insights from genomic heterogeneity. *Nature Reviews Genetics*, **14**, 179-190.
- 674 Li H, Durbin R (2009) Fast and accurate short read alignment with Burrows-Wheeler transform.  
675 *Bioinformatics*, **25**, 1754-1760.
- 676 Li H, Handsaker B, Wysoker A *et al.* (2009) The sequence alignment/map format and SAMtools.  
677 *Bioinformatics*, **25**, 2078-2079.
- 678 Li JT, Wang JS, Nian HH *et al.* (2015a) Amphibians crossing the bering land bridge: evidence from  
679 holarctic treefrogs (*Hyla*, Hylidae, Anura). *Molecular Phylogenetics and Evolution*, **87**, 80-90.
- 680 Li J, Zhao M, Wei SC *et al.* (2015b) Geologic events coupled with Pleistocene climatic oscillations  
681 drove genetic variation of Omei treefrog (*Rhacophorus omeimontis*) in southern China. *BMC  
682 Evolutionary Biology*, **15**, 289.
- 683 Li J, Wei SC, Hu ML *et al.* (2018) Reflection of paleoclimate oscillations and tectonic events in the  
684 phylogeography of moustache toads in southern China. *Journal of Zoology*, **305**, 17-26.
- 685 Liao WB, Lu X (2010) Age structure and body size of the Chuanxi Tree Frog *Hyla annectans*  
686 *chuanxiensis* from two different elevations in Sichuan (China). *Zoologischer Anzeiger-A  
687 Journal of Comparative Zoology*, **248**, 255-263.
- 688 Liu K (1988) Quaternary history of the temperate forests of China. *Quaternary Science Reviews*, **7**, 1-  
689 20.
- 690 Liu XM, Fu YX (2015) Exploring population size changes using SNP frequency spectra. *Nature  
691 Genetics*, **47**, 555-559.
- 692 McCormack JE, Hird SM, Zellmer AJ *et al.* (2013) Applications of next-generation sequencing to  
693 phylogeography and phylogenetics. *Molecular Phylogenetics and Evolution*, **66**, 526-538.
- 694 McKenna A, Hanna M, Banks E *et al.* (2010) The Genome Analysis Toolkit: a MapReduce framework  
695 for analyzing next-generation DNA sequencing data. *Genome Research*, **20**, 1297-1303.
- 696 Muscarella R, Galante PJ, Soley-Guardia M *et al.* (2014). ENMeval: An R package for conducting  
697 spatially independent evaluations and estimating optimal model complexity for Maxent  
698 ecological niche models. *Methods in Ecology and Evolution*, **5**, 1198-1205.
- 699 Newman CE, Austin CC (2016) Sequence capture and next generation sequencing of ultraconserved  
700 elements in a large genome salamander. *Molecular Ecology*, **25**, 6162-6174.
- 701 Oksanen FJ, Blanchet FG, Friendly M *et al.* (2019). *Vegan: Community ecology package*. R package  
702 version 2.5-6. <https://cran.r-project.org/package=vegan>
- 703 O'Rawe J, Jiang T, Sun GQ *et al.* (2013) Low concordance of multiple variant-calling pipelines:  
704 practical implications for exome and genome sequencing. *Genome Medicine*, **5**, 28.
- 705 Ovaskainen O, Karhunen M, Zheng CZ *et al.* (2011) A new method to uncover signatures of divergent  
706 and stabilizing selection in quantitative traits. *Genetics*, **189**, 621-632.
- 707 Owens HL, Campbell LP, Dornak LL *et al.* (2013) Constraints on interpretation of ecological niche  
708 models by limited environmental ranges on calibration areas. *Ecological Modelling*, **263**, 10-18.
- 709 Patterson N, Price AL, Reich D (2006) Population structure and eigenanalysis. *PLoS Genetics*, **2**, e190.
- 710 Phillips SJ, Anderson RP, Schapire RE (2006) Maximum entropy modeling of species geographic  
711 distributions. *Ecological Modelling*, **190**, 231-259.
- 712 Pickrell JK, Pritchard JK (2012) Inference of population splits and mixtures from genome-wide allele  
713 frequency data. *PLoS Genetics*, **8**, e1002967.
- 714 Puckett EE, Park J, Combs M *et al.* (2016) Global population divergence and admixture of the brown  
715 rat (*Rattus norvegicus*). *Proceedings of the Royal Society B: Biological Sciences*, **283**, 20161762.

716 R Core Team (2014) *R: A Language and Environment for Statistical Computing*. R Foundation for  
717 Statistical Computing, Vienna, Austria. <http://www.R-project.org/>

718 Raj A, Stephens M, Pritchard JK (2014) fastSTRUCTURE: Variational inference of population structure  
719 in large SNP data sets. *Genetics*, **197**, 573-589.

720 Rambaut A, Drummond AJ, Xie D, *et al.* (2018) Posterior summarization in Bayesian phylogenetics  
721 using Tracer 1.7. *Systematic Biology*, **67**, 901.

722 Reynolds RG, Fitzpatrick BM (2007) Assorted mating in poison-dart frogs based on an ecologically  
723 important trait. *Evolution*, **61**, 2253-2259.

724 Rudh A, Rogell B, Höglund J (2007) Non-gradual variation in color morphs of the strawberry poison  
725 frog *Dendrobates pumilio*: genetic and geographical isolation suggest a role for selection in  
726 maintaining polymorphism. *Molecular Ecology*, **16**, 4284-4294.

727 Sánchez-Montes G, Wang JL, Ariño AH *et al.* (2018) Mountains as barriers to gene flow in  
728 amphibians: Quantifying the differential effect of a major mountain ridge on the genetic structure  
729 of four sympatric species with different life history traits. *Journal of Biogeography*, **45**, 318-331.

730 Schoener TW (1968) The *Anolis* lizards of Bimini: Resource partitioning in a complex fauna. *Ecology*,  
731 **49**, 704-726.

732 Shen YH (1996) A new subspecies of *Hyla annectans* from Hunan, China (Anaura: Hylidae). *Zoological*  
733 *Research*, **18**, 177-182.

734 Shi YF, Ren B, Wang J, Derbyshire E (1986) Quaternary glaciation in China. *Quaternary Science*  
735 *Reviews*, **5**, 503-507.

736 Slatkin M (1995) A measure of population subdivision based on microsatellite allele frequencies.  
737 *Genetics*, **139**, 457-462.

738 Sokal RR, Rohlf FJ (1981) *Biometry*. W. H. Freeman and Co, San Francisco, USA.

739 Stange M, Sánchez-Villagra MR, Salzburger W *et al.* (2018) Bayesian divergence-time estimation with  
740 genome-wide single-nucleotide polymorphism data of sea catfishes (Ariidae) supports Miocene  
741 closure of the Panamanian Isthmus. *Systematic Biology*, **67**, 681-699

742 Sun BN, Wu JY, Liu YS *et al.* (2011) Reconstructing Neogene vegetation and climates to infer tectonic  
743 uplift in western Yunnan, China. *Palaeogeography Palaeoclimatology Palaeoecology*, **304**,  
744 328-336.

745 Sun XW, Liu DY, Zhang XF *et al.* (2013) SLAF-seq: an efficient method of large-scale *de novo* SNP  
746 discovery and genotyping using high-throughput sequencing. *PLoS ONE*, **8**, e58700.

747 Sun YB, Xiong ZJ, Xiang XY *et al.* (2015) Whole-genome sequence of the Tibetan frog *Nanorana*  
748 *parkeri* and the comparative evolution of tetrapod genomes. *Proceedings of the National*  
749 *Academy of Sciences USA*, **112**, E1257-E1262.

750 Wang HW, Ge S (2006) Phylogeography of the endangered *Cathaya argyrophylla* (Pinaceae) inferred  
751 from sequence variation of mitochondrial and nuclear DNA. *Molecular Ecology*, **15**, 4109-  
752 4122.

753 Wang GD, Zhang BL, Zhou WW *et al.* (2018) Selection and environmental adaptation along a path to  
754 speciation in the Tibetan frog *Nanorana parkeri*. *Proceedings of the National Academy of*  
755 *Sciences*, **115**, E5056-E5065.

756 Ward RD, Skibinsky DOF, Woodwark M (1992) Protein heterozygosity, protein structure and  
757 taxonomic differentiation. *Evolutionary Biology*, **26**, 3-131.

758 Warren DL, Glor RE, Turelli M (2008) Climate niche identity versus conservatism: Quantitative  
759 approaches to niche evolution. *Evolution*, **62**, 2868-2883.

760 Watanabe S, Hajima T, Sudo K *et al.* (2011) MIROC-ESM 2010: Model description and basic results  
761 of CMIP5-20c3m experiments. *Geoscientific Model Development*, **4**, 845-872.

762 Weaver AJ, Eby M, Fanning AF, Wiebe EC (1998) Simulated influence of carbon dioxide, orbital  
763 forcing and ice sheets on the climate of the Last Glacial Maximum. *Nature*, **394**, 847-853.

764 Xing YW, Ree RH (2017) Uplift-driven diversification in the Hengduan Mountains, a temperate  
765 biodiversity hotspot. *Proceedings of the National Academy of Sciences USA*, **114**, E3444-E3451.

766 Yan F, Zhou WW, Zhao HT *et al.* (2013) Geological events play a larger role than Pleistocene climatic  
767 fluctuations in driving the genetic structure of *Quasipaa boulengeri* (Anura: Dicroglossidae).  
768 *Molecular Ecology*, **22**, 1120-1133.



- 769 Ye Z, Zhu GP, Chen PP, Zhang DL, Bu WJ (2014) Molecular data and ecological niche modelling  
770 reveal the Pleistocene history of a semi-aquatic bug (*Microvelia douglasi douglasi*) in East Asia.  
771 *Molecular Ecology*, **23**, 3080-3096.
- 772 Zeisset I, Beebee TJC (2008) Amphibian phylogeography: a model for understanding historical aspects  
773 of species distributions. *Heredity*, **101**, 109-119.
- 774 Zhang RZ (1999) *Zoogeography of China*. Science Press, Beijing, China.
- 775 Zhao J, Shi Y, Wang J (2011) Comparison between Quaternary glaciations in China and the Marine  
776 Oxygen Isotope Stage (MIS): an improved schema. *Acta Geographica Sinica*, **66**, 867-884.
- 777 Zhao SC, Zheng PP, Dong SS *et al.* (2013) Whole-genome sequencing of giant pandas provides insights  
778 into demographic history and local adaptation. *Nature Genetics*, **45**, 67.
- 779 Zhao J, Perez MBM, Hu J, Fernandez MGS (2016) Genome-wide association study for nine plant  
780 architecture traits in Sorghum. *Plant Genome*, **9**, 2.
- 781 Zheng B, Xu Q, Shen Y (2002) The relationship between climate change and Quaternary glacial cycles  
782 on the Qinghai-Tibetan Plateau: review and speculation. *Quaternary International*, **97**, 93-101.
- 783 Zhou WJ, Yu XF, Jull AT *et al.* (2004). High-resolution evidence from southern China of an early  
784 Holocene optimum and a mid-Holocene dry event during the past 18 000 years. *Quaternary*  
785 *Research*, **62**, 39-48.
- 786 Zhou XM, Meng XH, Liu ZJ *et al.* (2016) Population genomics reveals low genetic diversity and  
787 adaptation to hypoxia in snub-nosed monkeys. *Molecular Biology and Evolution*, **33**, 2670-  
788 2681.

#### 789 **Data Accessibility**

790 Aligned datasets, all ascii files from the SDM along with the all morphological data deposited in Dryad  
791 ([https://datadryad.org/stash/share/TvAr1XyODIzwAfP6zV4\\_7sow-2ucxSr85T9Dfo4RcxY](https://datadryad.org/stash/share/TvAr1XyODIzwAfP6zV4_7sow-2ucxSr85T9Dfo4RcxY)). Sampling  
792 locations and additional individuals included in SDM analyses are uploaded as online Supporting  
793 Information. All raw sequence data are uploaded to Genbank's Short Read Archive (Accession nos.  
794 SRR12349892–SRR12350250).

#### 795 **Author contributions**

796 H.W., J.M.: designed the research and contributed to draft the manuscript. C.F.: contributed to sampling  
797 of materials. S.W., Z.L. and P.M.: analyzed the data. S.W., P.M. and J.M. interpreted the results. S.W.  
798 wrote the manuscript with significant contributions from other authors. All authors read and approved  
799 the final manuscript.

#### 800 **Conflicts of interest**

801 Authors declare no conflict of interests

802 **Tables and Figures**

803 **Table 1.** Results of dbRDA analysis testing for the effect of geographic (GEO1-3, Elevation) and  
 804 environmental (BIO1, BIO2, BIO12, BIO14) on the degree of genetic differentiation (as measured by  
 805  $F_{ST}$ ) among 35 populations of *H. annectans*. See text for explanation of GEO and BIO variables.

	% of variance explained	<i>d.f.</i>	<i>F</i>	<i>P</i>
Geography	0.37			
Elevation	0.14	1	5.34	0.001
GEO1	0.13	1	4.82	0.001
GEO2	0.08	1	3.04	0.001
GEO3	0.02	1	0.81	0.597
Environment	0.41			
BIO1	0.06	1	2.12	0.033
BIO2	0.13	1	5.01	0.002
BIO12	0.08	1	2.73	0.004
BIO14	0.14	1	5.39	0.001
Residual	0.22	26		

806

807 **Table 2.** Summary of niche divergence comparisons among five *H. annectans* lineages using  
 808 Schoener's *D* (above diagonal) and Warren's *I* (below diagonal).

Lineages	N1	N2	W	C	E
	Schoener's <i>D</i>				
N1	1.000	0.337	0.542	0.230	0.154
N2	0.634	1.000	0.394	0.377	0.118
W	0.831	0.679	1.000	0.456	0.238
C	0.511	0.653	0.774	1.000	0.438
E	0.370	0.296	0.488	0.745	1.000

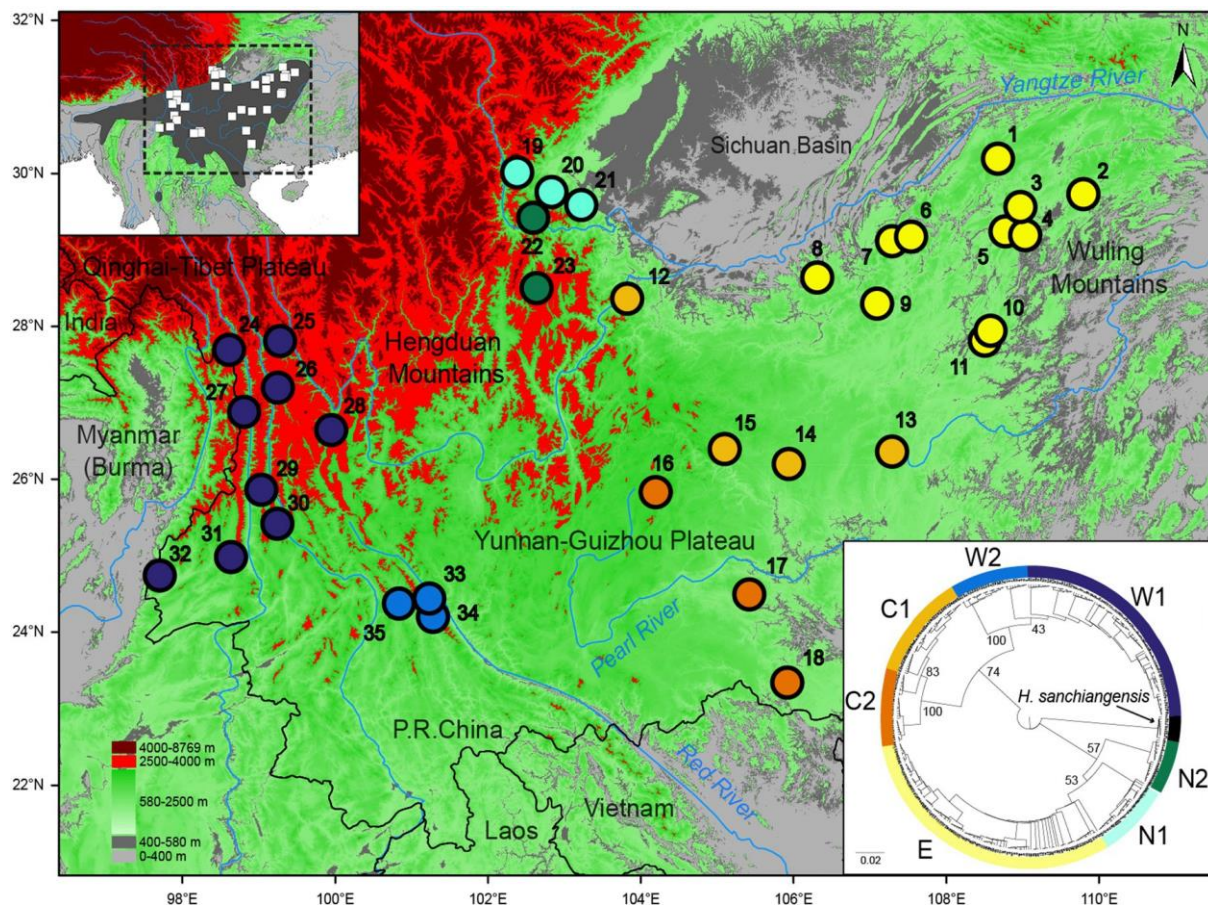
809

810 **Table 3.** Results of Kruskal-Wallis and subsequent *post hoc* (Dunn's multiple comparisons test) tests  
 811 for differences in mean number of black spots among the seven main *H. annectans* lineages.

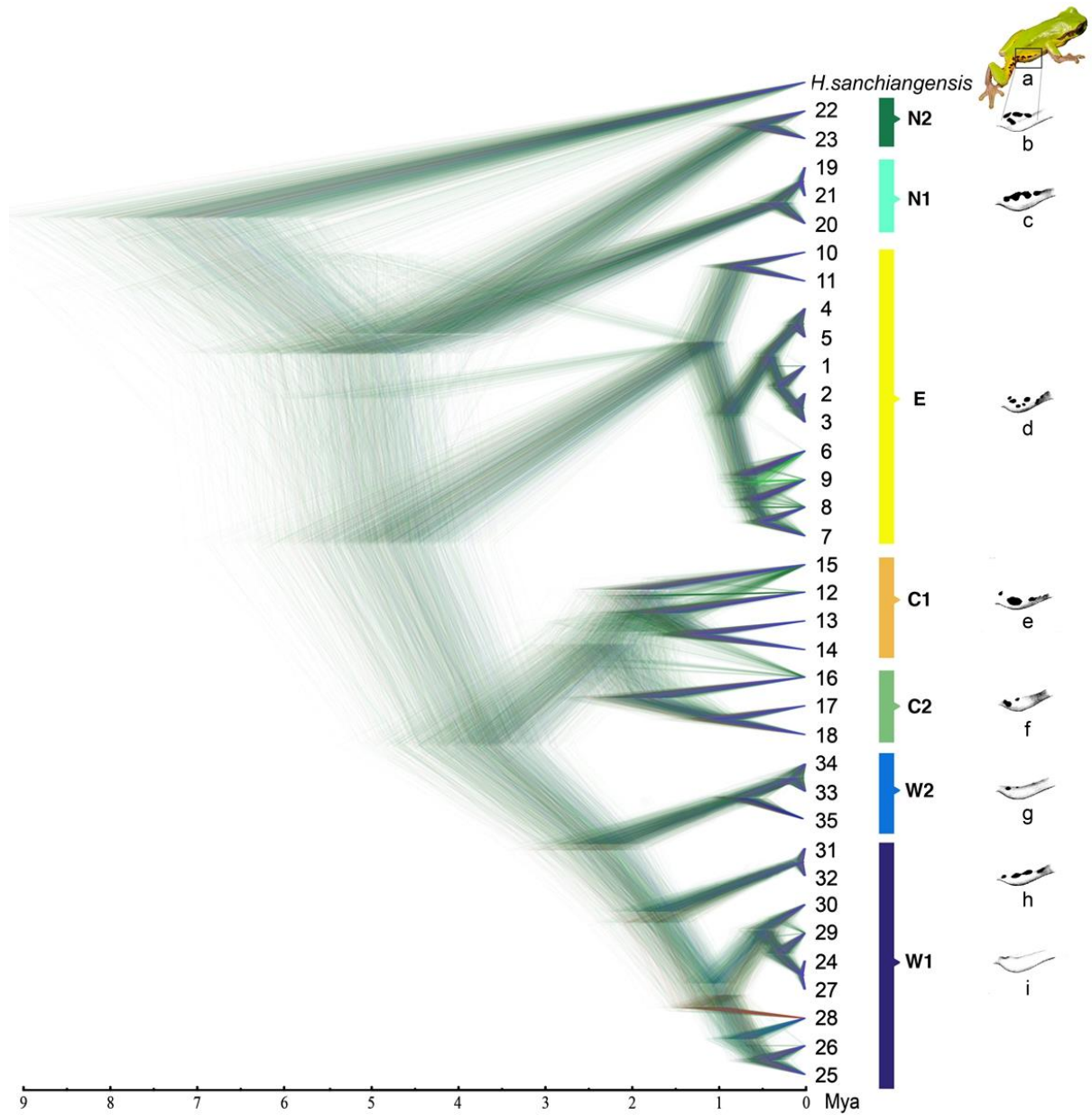
Lineage	N	Mean rank	Kruskal-Wallis test value	<i>P</i>	Dunn's multiple comparison test					
					C1	C2	N1	N2	W1	W2
E	100	281.30	258.22	<0.001	*	*	*	*	*	*
C1	40	202.13				*	ns	ns	*	*

C2	30	112.25	ns	ns	ns	ns
N1	29	187.03		ns	*	ns
N2	20	158.50			*	ns
W1	90	67.62				ns
W2	30	112.25				

812 \*  $P < 0.05$

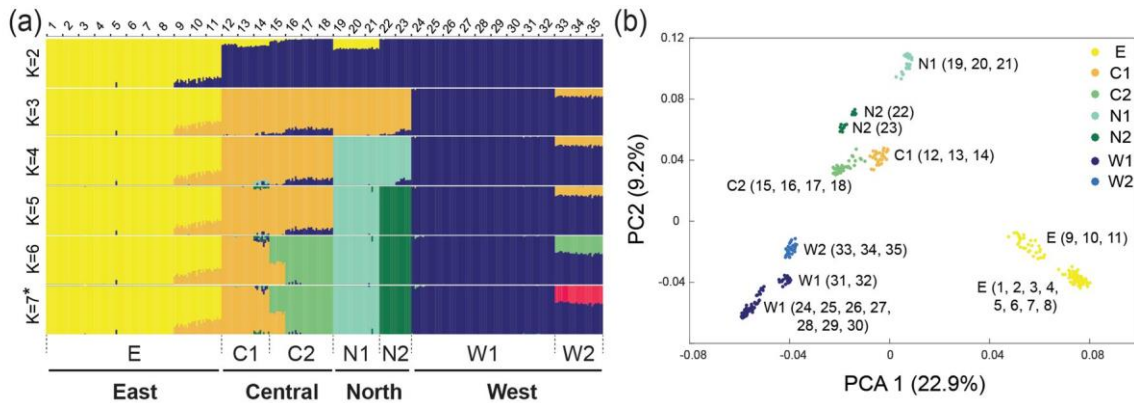


813  
814 **Figure 1.** Thirty five sampling sites of 349 *H. annectans* individuals from southern China (black  
815 symbols). The grey shade in the left corner insert indicates the entire species distribution range,  
816 downloaded from the IUCN website (<http://www.iucnredlist.org/>). The primary mountain systems and  
817 basins are indicated, and the major rivers are depicted with blue lines. The gradient of color on the map  
818 represents different elevations, the areas exceeding values suitable for *H. annectans* are shown in red  
819 (high elevation) and grey (low elevation). Populations are numbered as in Table S1. The phylogenetic  
820 tree on the right corner insert is a NJ tree constructed in MEGA X, branch labels represent bootstrap  
821 support value. Seven genetic lineages are indicated with different colors, which are also used in all other  
822 figures.



823  
824  
825  
826  
827  
828  
829  
830  
831  
832  
833  
834

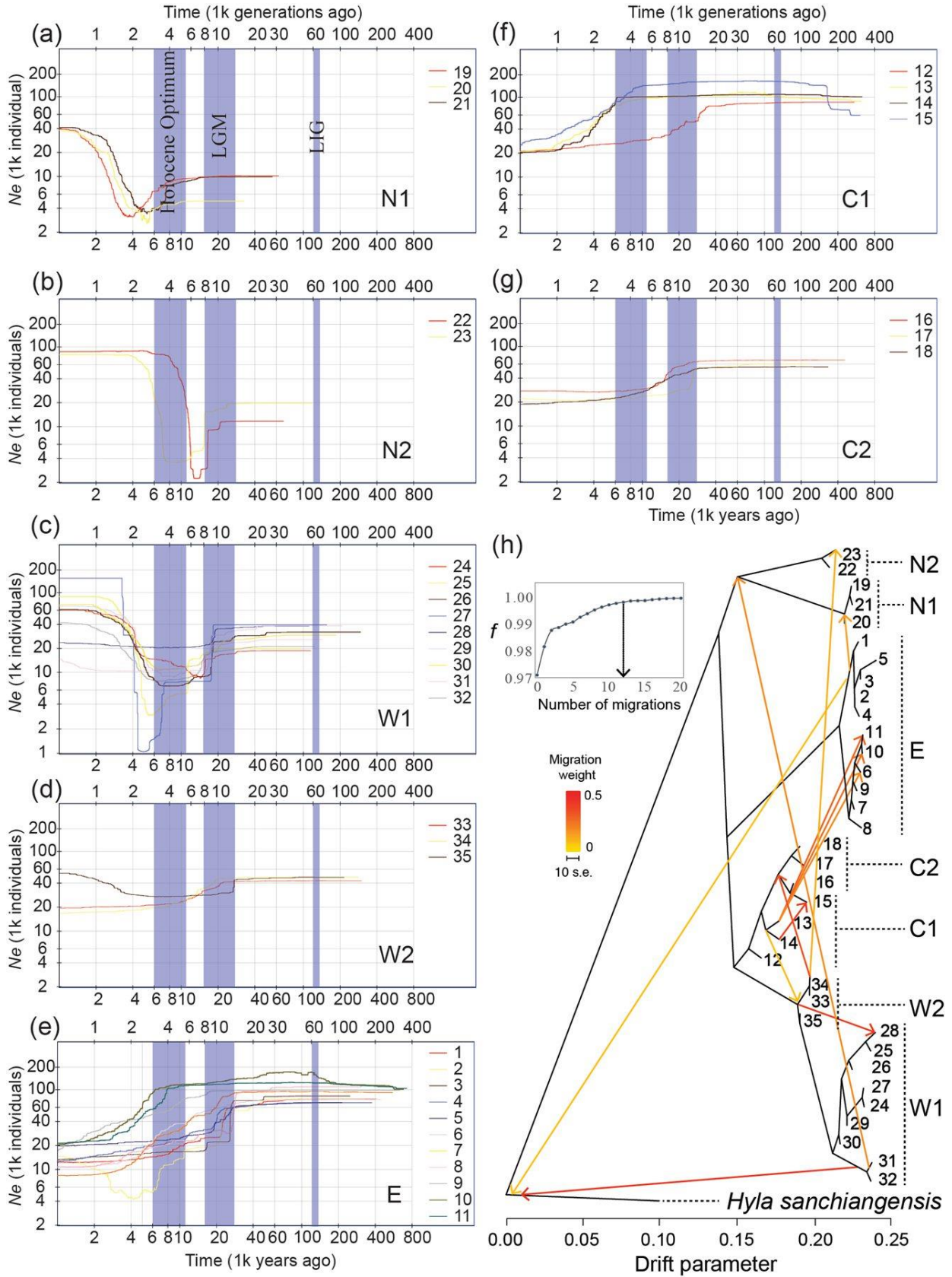
**Figure 2.** Phylogenetic relationships and phenotypic variation among *H. annectans* lineages. The SNAPP tree was obtained using *H. sanchiangensis* as an outgroup. Divergence times are shown on the horizontal axis. Colored boxes highlight the seven lineages consistent with genetic clustering analyses. The number of black spots on flanks is given on the right: a, *H. annectans* (this individual was not included in this study); b, individual “fp” from site 22 and genetic cluster N2 (4 black spots); c, individual “fg” from site 19 and genetic cluster N1 (4 black spots); d, individual “bf” from site 11 and genetic cluster E with (7 black spots); e, individual from site 14 and genetic cluster C1 (3 black spots); f, individual “ku” from site 18 and genetic cluster C2 (2 black spots); g, individual “lq” from site 35 and genetic cluster W2 (2 black spots); h, individual “nk” from site 31 and genetic cluster W1 (4 black spots); i, individual “jg” in site 27 and genetic cluster W1 (no black spots).



835  
836  
837  
838  
839  
840

**Figure 3.** Inferred genetic structure of *H. annectans* populations according to (a) Bayesian cluster analysis using fastSTRUCTURE from  $K = 2$  to  $K = 7$  based on the 8,420 SNP dataset, and (b) PCA based on the 8,420 SNP dataset. In (a), codes above and below the plot refer to population and cluster identifiers, respectively. Different clusters are indicated with different colors. \*denotes the optimal  $K$  value. In (b) the different colors of individual data points are coded according to their cluster identities.

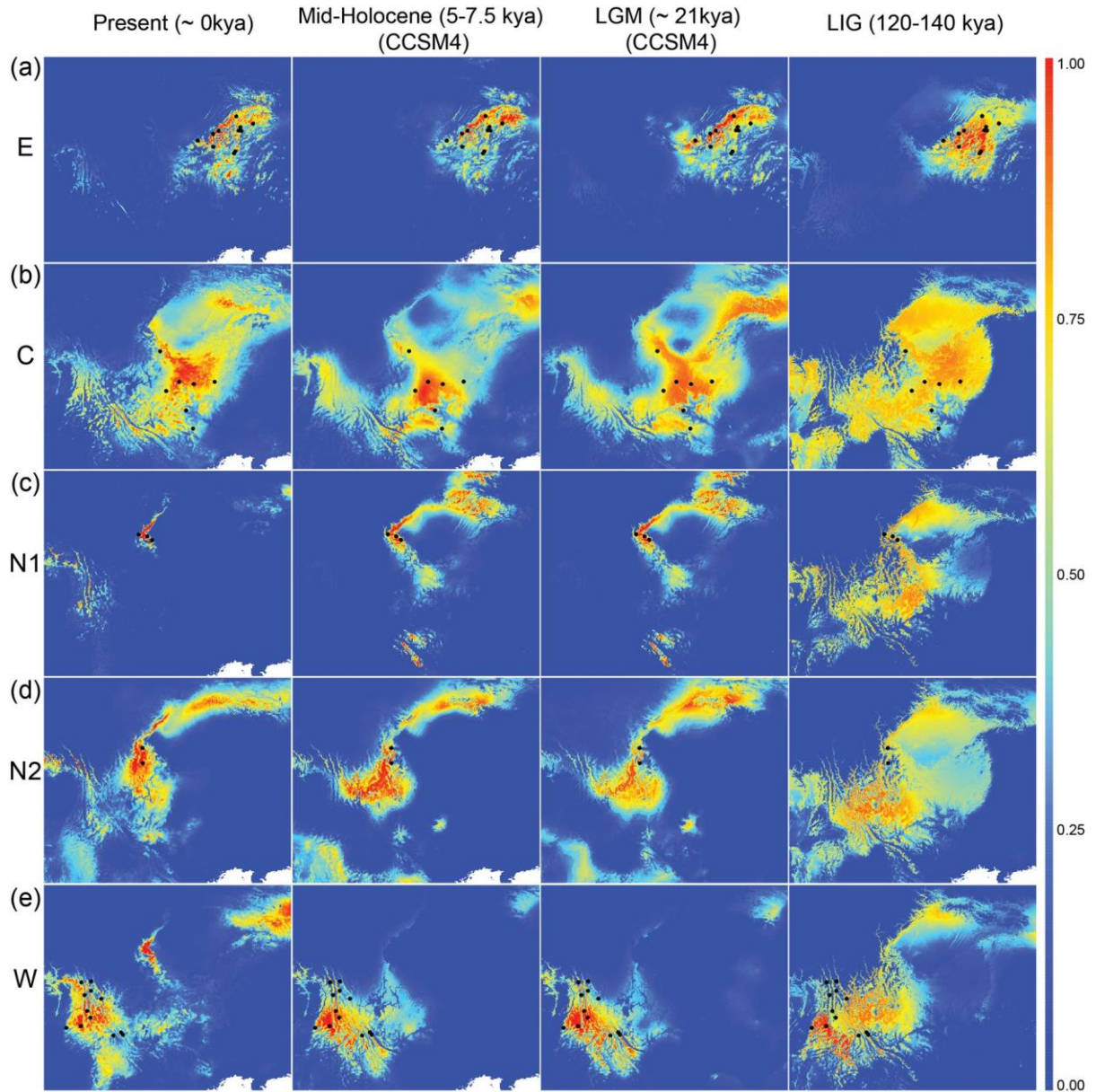




842  
843  
844  
845

**Figure 4.** Demographic history of *H. annectans* lineages. The x-axis indicates time, and the y-axis indicates  $N_e$ . Different colored lines in the plot depict different populations within a given lineage. (a) to (g) are STAIRWAY PLOTS for populations of the N1, N2, W1, W2, E, C1 and C2 lineages,

846 respectively. The blue shaded areas mark the Holocene Optimum (6–11 Kya, constrained by Zhou *et al.*  
 847 2004), LGM (16–28 kya, constrained by Zhao *et al.* 2011) and LIG (120–140 kya, WorldClim:  
 848 <http://www.worldclim.org/>) periods. (h) Migration among lineages inferred by TREEMIX. The  
 849 migration weight indicates the proportion of ancestry derived from the migration edge.  
 850



851  
 852 **Figure 5.** Species distribution models for *H. annectans* for present and historical (Mid Holocene (5–7.5  
 853 kya), Last Glacial Maximum [LGM], 21 kya and the Last Interglacial [LIG], 120–140 kya) times.  
 854 Warmer colors indicate higher probability of occurrence as predicted by MAXENT (Phillips *et al.*  
 855 2006). Black symbols depict sampling sites used in this study. (a) to (e) are SDMs for populations of  
 856 the E, C, N1, N2, and W lineages, respectively.

857 **Supporting information**

858 Additional supporting information may be found in the online version of this article:

859 **Table S1.** Sampling site data, gender and distribution cluster for genetic samples of *H. annectans* used  
860 in this study.

861 **Table S2.** Summary of each dataset used for the respective analysis.

862 **Table S3.** GPS points used for building species distribution models for *H. annectans*.

863 **Table S4.** Bioclimatic variable selection for species distribution modelling based on PCA analysis.

864 **Table S5.** Summary of SLAF data collected in the final assembly of 349 samples of *H. annectans*.

865 **Table S6.** Summary statistics of average observed heterozygosity ( $H_o$ ), average expected  
866 heterozygosity ( $H_e$ ) and pairwise  $F_{ST}$  values between the 35 populations of *H. annectans*. All  $F_{ST}$  values  
867 are statistically significant ( $P < 0.05$ ).

868 **Table S7.** Best fit MAXENT model based upon delta AICc from ENMeval.

869 **Table S8.** AUC values for each model.

870 **Table S9.** Pairwise  $F$ -values of morphological features (snout-vent length [SVL] and weight) of 339  
871 individuals from the seven main genetic lineages of *H. annectans*. Data were analyzed with Welch  
872 ANOVA using a Games-Howell *post hoc* test.

873 **Figure S1.** SNAPP tree with the 95% posterior distributions of the time calibration.

874 **Figure S2.** Results from fastSTRUCTURE clustering analyses using the simple models. (a) Prediction  
875 error from five-fold cross-validation. The lowest value of CV error is when  $K = 7$ . (b) The marginal  
876 likelihood at increasing number of  $K$ . The marginal likelihood is maximized when  $K = 7$ .

877 **Figure S3.** Genetic isolation by distance.

878 **Figure S4.** Variance partitioning results of dbRDA analyses.

879 **Figure S5.** Delta AICc values of all models compared in ENMeval.

880 **Figure S6.** SDMs for other models.

881 **Figure S7.** Mobility-oriented parity analysis with during three periods (HM, LGM, and LIG).



**Supporting Information for:**

**The roles of climate, geography and natural selection as drivers of genetic and phenotypic differentiation in a widespread amphibian *Hyla annectans* (Anura: Hylidae)**

Shichao Wei<sup>1</sup>, Zitong Li<sup>2</sup>, Paolo Momigliano<sup>2</sup>, Chao Fu<sup>1</sup>, Hua Wu<sup>1\*</sup>, & Juha Merilä<sup>2</sup>

<sup>1</sup>*Institute of Evolution and Ecology, School of Life Sciences, Central China Normal University, 152 Luoyulu, Hongshan District, 430079 Wuhan, China*

<sup>2</sup>*Ecological Genetics Research Unit, Organismal and Evolutionary Biology Research Programme, Faculty of Biological and Environmental Sciences, University of Helsinki, P.O. Box 65, FI-00014 Helsinki, Finland*

**Corresponding author:** Hua Wu, [wuhua@mail.ccnu.edu.cn](mailto:wuhua@mail.ccnu.edu.cn)

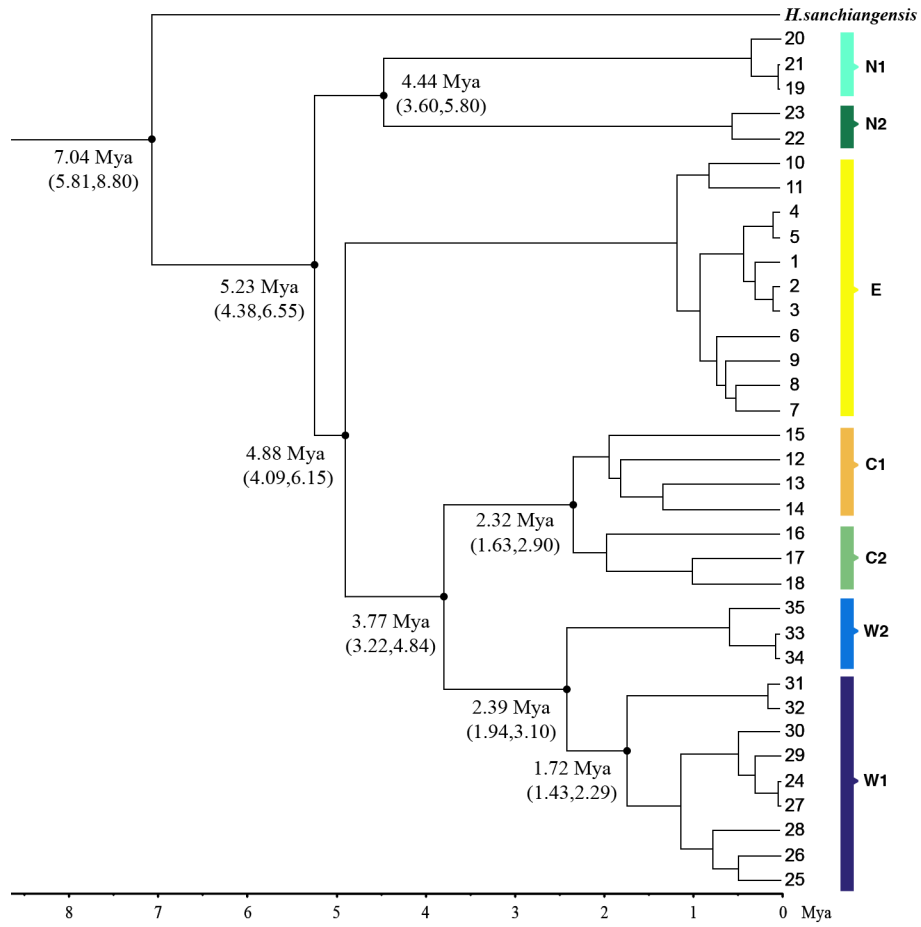


**Figure S1.** SNAPP tree illustrating phylogenetic relationships among *H. annectans* using *H. sanchiangensis* as an outgroup. The lineage divergence times were calibrated and the numbers in the brackets represent the 95% posterior distributions of the estimates. Colored boxes highlight the seven lineages consistent with genetic clustering analyses.

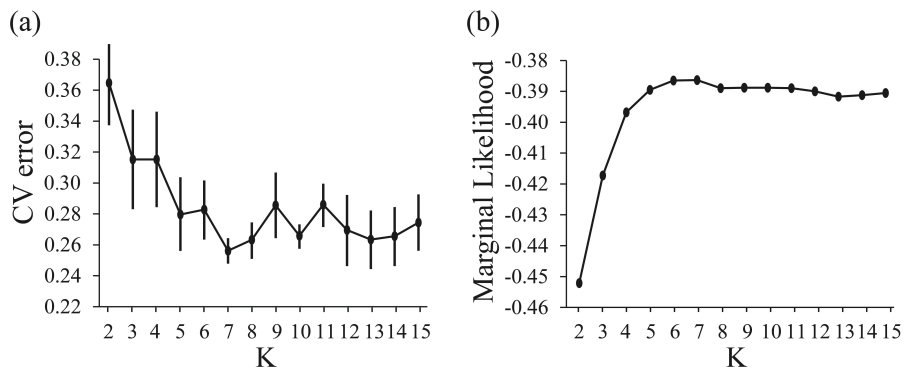


**Figure S2.** Results from fastSTRUCTURE clustering analyses using the simple model. (a) Prediction error from fivefold cross-validation (CV) for the fastSTRUCTURE analyses, the lowest value of CV error is when  $K = 7$ . (b) The marginal likelihood at increasing number of  $K$ . The marginal likelihood is maximized when  $K = 7$ .

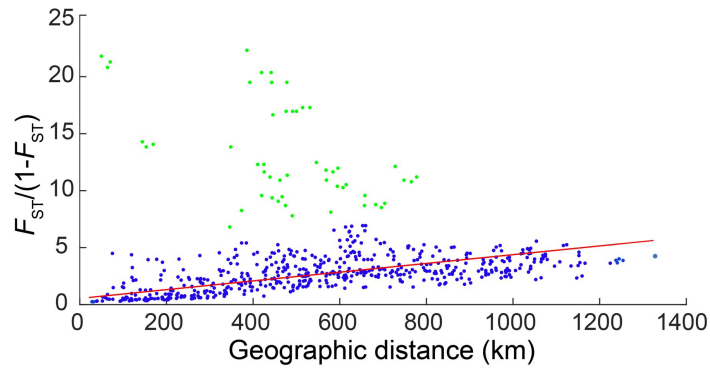


**Figure S3.** Correlation between pairwise genetic differentiation among populations (Slatkin's linearized  $F_{ST}$ ) and the geographic distance separating populations. The green dots indicate comparisons of populations in clusters N1, N2 and W1, and were excluded from the other correlation analysis. The red line is the slope of linear regression (excluding the green data points) given solely for illustrative purposes.

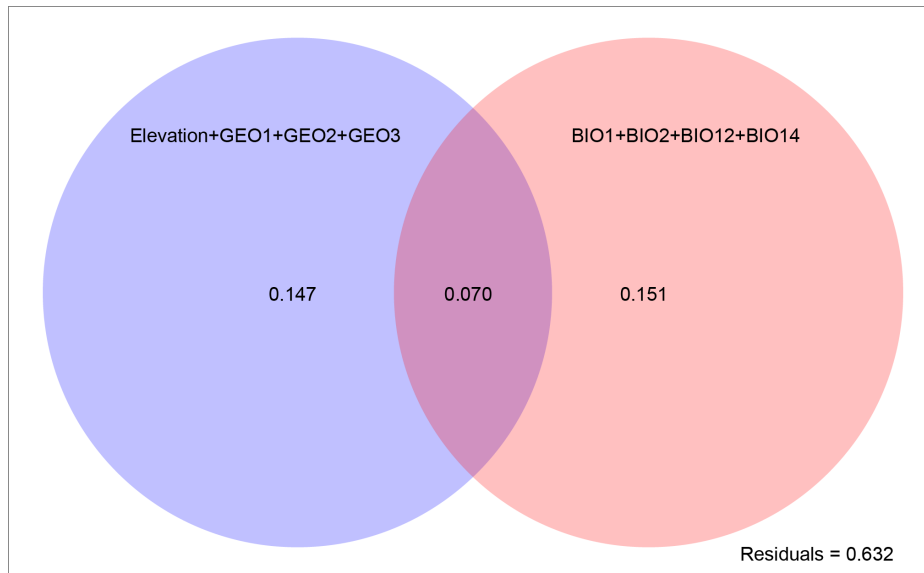


**Figure S4.** Variance partitioning results of dbRDA analyses. Geographic variables comprises four geographic vectors (Elevation, GEO1, GEO2, GEO3). Environmental variables comprise four environmental variables: BIO1, BIO2, BIO12, BIO14.

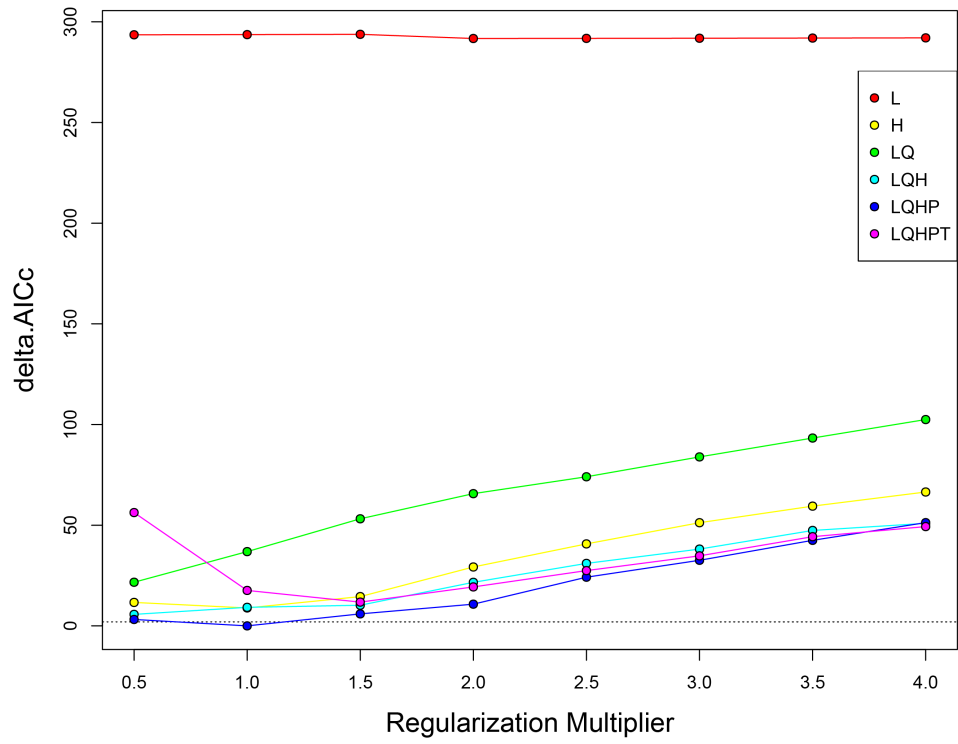


**Figure S5.** Delta AICc values of all models compared in ENMeval, model LQHP 1 was the best fit model.

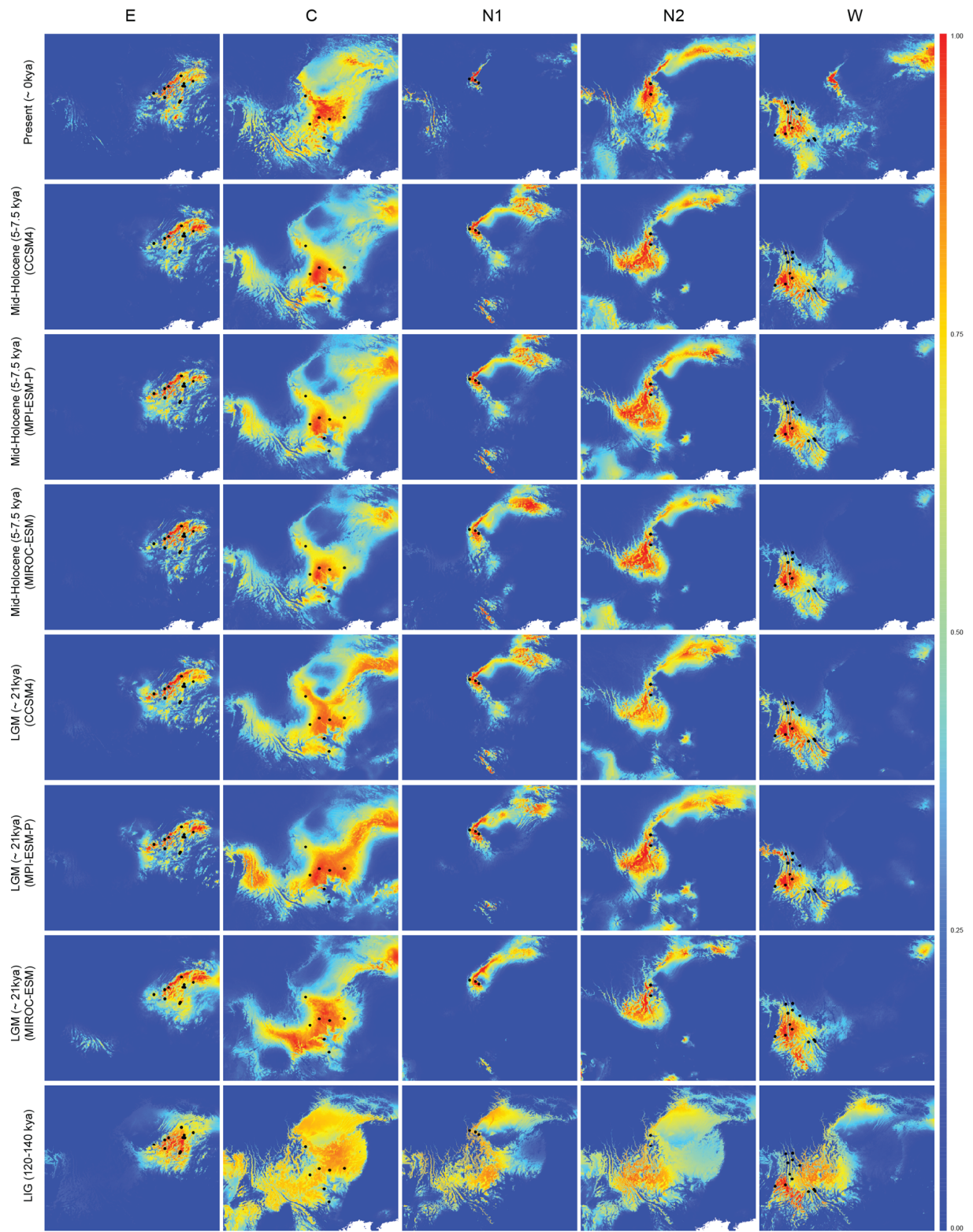


**Figure S6.** SDM for other models.

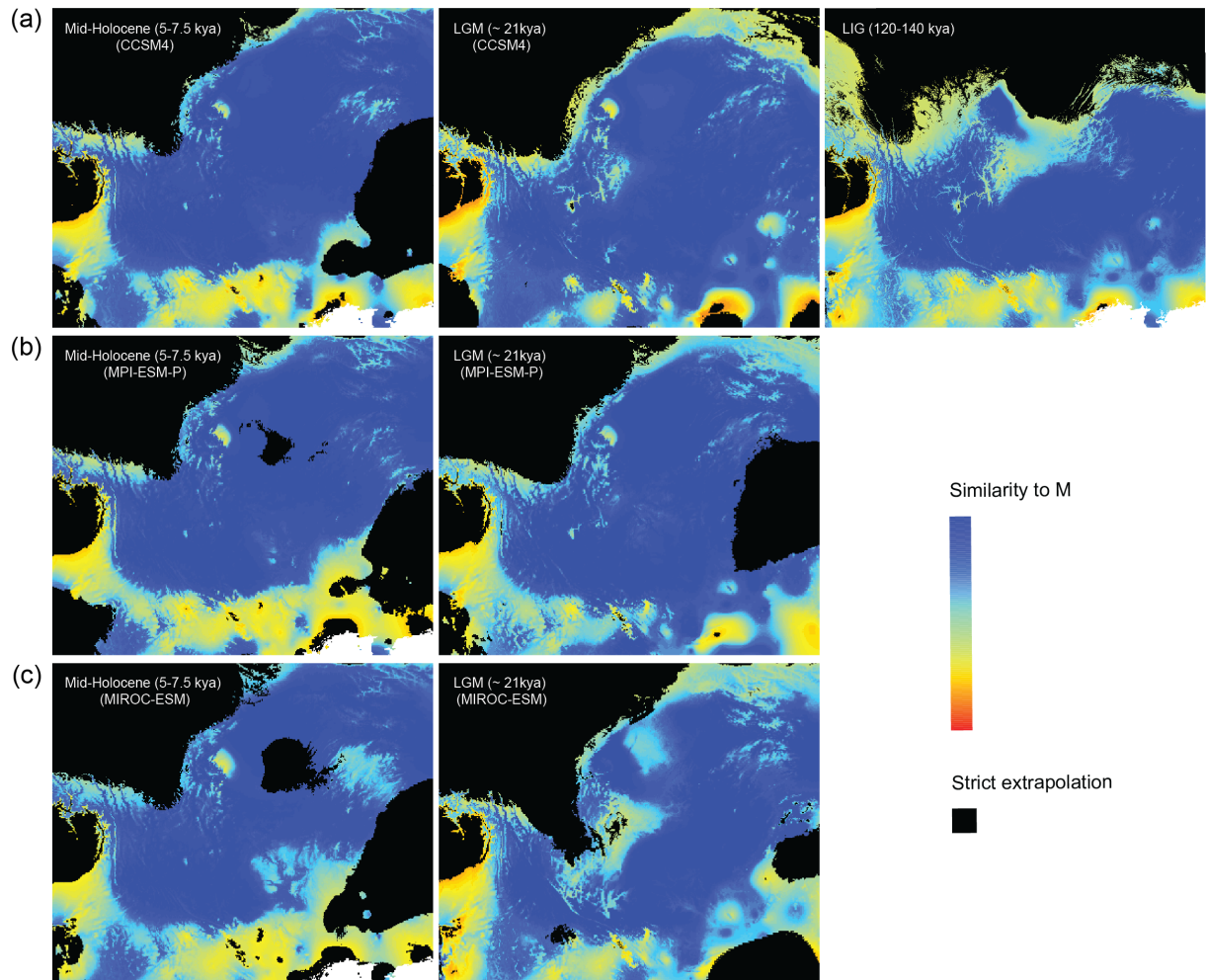


**Figure S7.** Mobility-oriented parity analysis comparing current conditions of the calibration region for *H. annectans* distribution modelling during three periods (MH, LGM, and LIG). (a) Results for the CCSM4 scenario. (b) Results for MPI-ESM-P and (c) the results for MIROC-ESM. Blue indicates similar climates to the current climate. Black indicates areas of strict extrapolation.

**Table S9.** Pairwise  $F$ -values of morphological features (snout-vent length [SVL] and weight) of 339 individuals from the seven g were analyzed with Welch ANOVA using a Games-Howell *post hoc* test.

	SVL	Weight	SVL	Weight	SVL	Weight	SVL	Weight	SVL
Cluster C1	0,903	0,354							
Cluster C2	1,144	0,447*	0,240	0,093					
Cluster N1	0,160	0,333	1,064	0,687*	1,304	0,78*			
Cluster N2	0,215	0,263	1,119	0,617	1,359	0,71*	0,055	0,070	
Cluster W1	0,629	0,222	1,533	0,576*	1,773*	0,669*	0,469	0,111	0,415
Cluster W2	0,052	0,020	0,956	0,373	1,196	0,467*	0,108	0,313	0,163

\*  $P < 0.05$

genetic lineages of *H. annectans*. Data

---

Weight	SVL	Weight
0,040		
0,243	0,578	0,202

---